The dynamics of forearc – back-arc vertical motion: numerical models and observations from the Mediterranean

A. Balázs[1], C. Faccenna[2,3], T. Gerya[1], K. Ueda[1], and F. Funiciello[2]

[1]ETH Zürich, Department of Earth Sciences, Zürich, Switzerland

[2]Università Roma Tre, Department of Sciences, Rome, Italy

[3]GFZ Potsdam, Germany.

Corresponding author: Attila Balázs (attila.balazs@erdw.ethz.ch)

Key Points:

- Evolution of forearc basins controlled by slab advance and steepening
- Subsidence of back-arc basins controlled by slab roll-back and mantle flow
- Insights into the evolution of Mediterranean forearc and back-arc basin systems

Graphical abstract

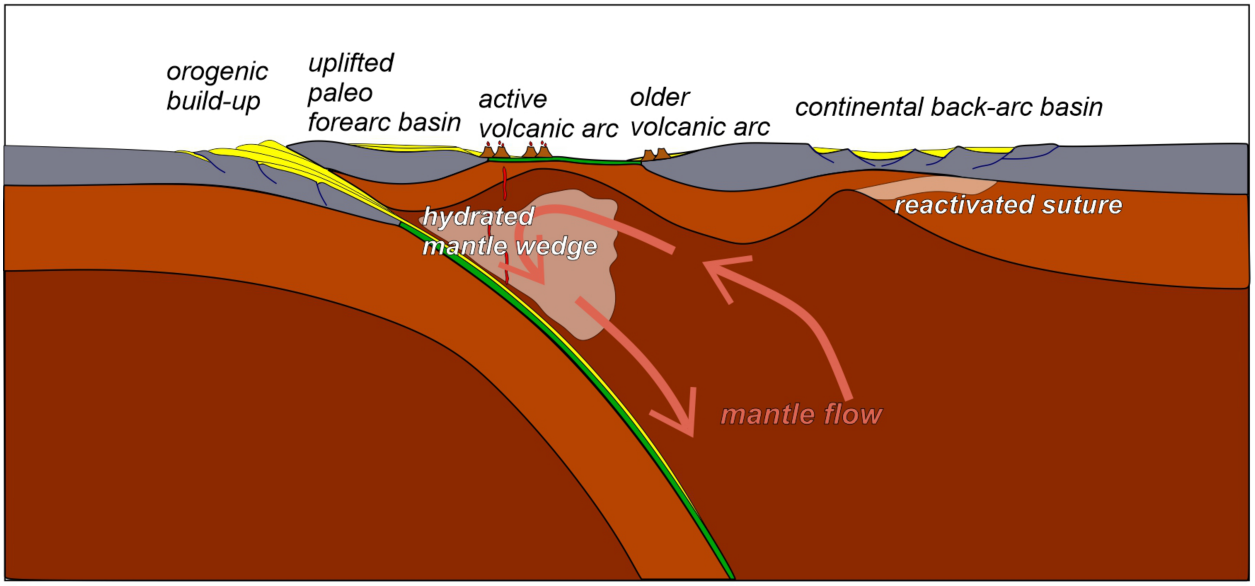

Abstract

The evolution of subduction zones influences the rise and demise of forearc and back-arc basins on the overriding plate. We conducted 2D elasto-visco-plastic numerical models of oceanic subduction and subsequent continental collision which include erosion, sedimentation, and hydration processes. The models show the evolution of wedge-top and retro-forearc basins in the continental

overriding plate, separated by a forearc high. These forearc regions are affected by repeated compression and extension phases. Higher subsidence rates are recorded in the syncline structure of the retro-forearc basin when the slab dip angle is higher and the subduction interface is stronger and before the slab reaches the 660 km upper-lower mantle discontinuity. The 3-4 km negative residual topographic signal is produced by the gradually steepening slab, which drags down the overlying upper plate. Extensional back-arc basins are either formed along inherited crustal or lithospheric weak zones at large distance from the arc region or are created above the hydrated mantle wedge originating from arc rifting. Back-arc subsidence is primarily governed by crustal thinning controlled by slab roll-back. Onset of collision and continental subduction is linked to the rapid uplift of the forearc basins; however, the back-arc region records ongoing extension during the initial phase of soft collision. Finally, during subsequent hard collision both the forearc and back-arc basins are ultimately affected by compression. Our modelling results provide insights into the evolution of Mediterranean subduction zones and propose that the Western-Eastern Alboran, Paola-Tyrrhenian, Transylvanian-Pannonian Basins should be considered as genetically connected forearc –back-arc basins, respectively.

1. Introduction

The topography and thermal history of the Earth are controlled by the inherent links between lithospheric and crustal tectonics, mantle convection and surface processes, such as erosion and sedimentation coupled to climatic variations (Burov, 2011; Whipple, 2009). Topography is mostly governed by isostasy, depending on crustal and lithospheric density (Holmes, 1944). However, along subduction zones the topography of the overriding plate strikingly differ from isostatic predictions, producing kilometer-scale residual non-isostatic topographic signals (Braun, 2010; Flament et al., 2013; Faccenna and Becker, 2020). Geodynamic models illustrate the potential contribution of different parameters on the topography and gravity signal of subduction zones (e.g., Billen and Gurnis, 2001; Buiter et al., 2001; Crameri et al., 2017; Davies, 1981; Espurt et al., 2008; Husson et al., 2012; Pusok and Kaus, 2015; Sizova, 2010; Vogt et al., 2012; Zhong and Gurnis, 1992). However, several subduction zone margins show sudden changes of their vertical motions that are still enigmatic, and the origin of related sedimentary basins is still poorly understood.

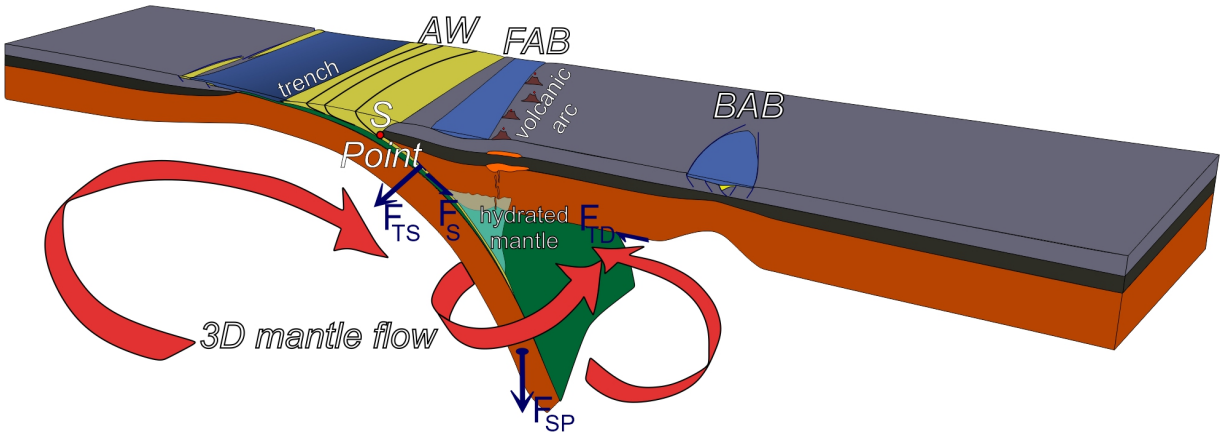

Figure 1. Simplified sketch of a subduction zone, forearc (FAB) and back-arc (BAB) basins and their main driving forces. Sediments are partly accumulated in the trench building up the accretionary wedge (AW) and are partly subducted deeper. F_{TS} – trench suction force acting within the subduction interface along the base of the upper plate connected to the downward suction of the lower plate (Forsyth and Uyeda, 1975). F_{SP} – slab pull force acting on the slab. F_{TD} – Force generated by the trench-ward mantle drag acting on the base of the upper plate. F_S – Shear force acting on the base of the upper plate driven by the subducting plate. Subduction is inherently linked to mantle flow around the slab. S-point – singularity point marking the upper edge of the upper and lower plate contact.

Sedimentary basins formed on the upper plate of subduction zones are commonly classified into forearc and back-arc basins based on their position with respect to the active volcanic arc (Fig. 1; Karig, 1971). Forearc basins overlying the landward side of the accretionary wedge are often called wedge-top forearc basins, while depocenters being formed on the overriding plate are classified as retro-forearc basins (Fuller et al., 2006; Noda, 2016; Mannu et al., 2017). Stratigraphic interpretation of these basins inferred repeated phases of extension and contraction superimposed on the overall convergent margin evolution, accretionary wedge growth and seal-level variations (Moore et al., 2015; Mannu et al., 2017; Menant et al., 2020). Furthermore, the observed 1.5-5 km negative residual topography that cannot be solely accommodated by crustal-scale faults are often linked to downward mantle flow or downward suction of the oceanic slab (Dickinson and Seely, 1979).

Extensional stress is supposedly linked to trench retreat and slab roll-back coupled to mantle flow towards the retreating slab (e.g., Forsyth and Uyeda, 1975; Wallace et al., 2009). Extensional deformation and crustal thinning are localized along weak zones either along the volcanic arc leading to arc rifting and spreading that migrates in the direction of slab retreat (Karig, 1971; Dymkova et al. 2016) or flanking collisional zones (Wallace et al., 2009; Li et al., 2013). Further-

more, continental back-arc extension is often localized at larger distances along inherited crustal or lithospheric structures (e.g., Shemenda, 1993; Dal Zilio et al., 2018; Yang et al., 2021). Subsidence and uplift patterns of the forearc and back-arc regions are influenced by a wide range of parameters that are linked to the stress transfer from the subducting plate towards the upper plate through the mantle wedge and subduction interface (Billen and Gurnis, 2001), vertical stresses created by the underlying mantle flow (Husson, 2006), rheological properties of the downgoing and upper plates (Conrad and Hager, 1999; Capitanio et al., 2010; Andric et al., 2018; Wolf and Huismans, 2019) and the strength of the subduction fault (Zhong and Gurnis, 1994) and their links to erosion and sedimentation (Behr and Becker, 2018; Sobolev and Brown, 2019; Brizzi et al., 2020; Balázs et al., 2021a).

Understanding the above-mentioned processes requires an integrated approach involving a high-resolution, coupled thermo-mechanical model handling elasto-visco-plastic rheologies of the crust and mantle and simulating erosion, sedimentation, and topographic evolution. In this study we aim to quantify forearc and back-arc basin forming mechanisms and their subsidence history during oceanic subduction and subsequent continental collision by means of numerical forward modelling, constrained by observational data from the Carpathians, Calabrian and Gibraltar subduction zones within the Mediterranean region. We conducted a parametric study testing systematically the influence of inherited crustal and lithospheric weak zones in the overriding plate, the role of different kinematic conditions and different sedimentation rates on upper plate deformation and topographic evolution.

1. Methods

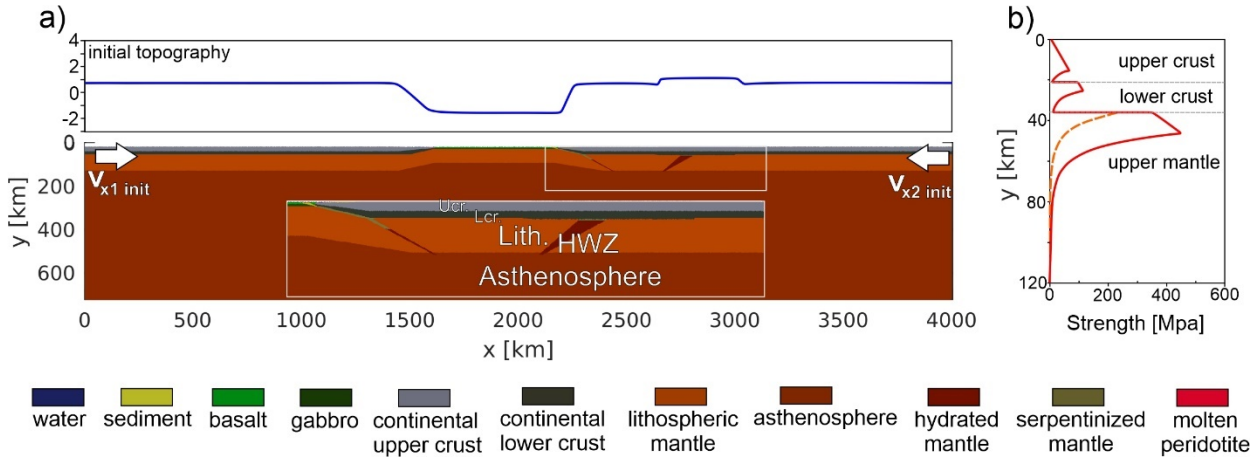

Figure 2. Initial model setup. a) 2D domain is resolved by 1361 × 283 nodal points, with more than 7 million randomly distributed markers. The model domain consists of a continental overriding plate and a subducting plate including both oceanic and continental lithosphere. An inclined weak zone of wet olivine

rheology is defined along one edge of the ocean to initiate subduction. Additional hydrated weak zone (HWZ) is defined in the overriding plate representing an inherited suture zone. b) Initial strength profile of the continental overriding plate (assuming constant strain rate of 10^{-14} s^{-1}). Red line indicates the laterally homogenous lithosphere, orange dashed line corresponds to the hydrated weaker lithosphere.

2.1 Numerical method description

The 2D numerical models are conducted with the thermomechanical code I2ELVIS, which solves the mass, momentum, and energy conservation equations on an Eularian staggered grid, using finite differences and marker-in-cell techniques (Gerya and Yuen, 2007). Solving the energy equation including latent, adiabatic, radiogenic and shear heat production simulates the thermal evolution of the model. Physical properties are transported by Lagrangian markers that move with the velocity field interpolated from the fix grid. The model incorporates effects that are essential for the study of subduction and upper plate deformation and topographic evolution. The code uses non-Newtonian elasto-visco-plastic rock rheologies (Table 1) and models in a simplified manner aqueous fluid transport and hydration/dehydration processes. The initial model setup assumes pore water in sediments and basaltic crust and mineral bound water in sediments, basaltic crust and gabbroic crust. Linear pore water release is assumed from 0 to 75 km depth. Bound water release is calculated by free-energy minimization as a function of pressure, temperature and rock type (Gerya and Yuen, 2007; Gerya and Meilick, 2011).

	Upper cont. crust	Lower cont. crust	Lithospheric mantle	B
Thickness (km)	20	15	75	3
Rheology	wet quartzite	plagioclase	dry olivine	p
Density, $_0$ (kg m^{-3})	2750	3000	3300	3
Pre-exponential factor, $1/A_D$ (Pa^n s)	1.97×10^{17}	4.8×10^{22}	3.98×10^{16}	4
Activation energy, E (kJ mol^{-1})	154	238	532	2
Power law exponent, n	2.3	3.2	3.5	3
Cohesion (Pa)	3×10^6	3×10^6	3×10^6	3
Coefficient of friction, sin( )	0.3-0.1	0.3-0.1	0.6-0.3	0
Radioactive heat production, H_r (W/m^3)	2	0.2	0.022	0

Table 1. Main parameters of the numerical models.

Surface processes, such as erosion and sedimentation are simulated at each timestep by the following transport equation:

$$\frac{\partial y_{\text{surf}}}{\partial t} = v_y - v_x \frac{\partial y_{\text{surf}}}{\partial x} - v_{\text{sedim}} + v_{\text{erosion}}$$

where y_{surf} is the vertical position of the surface as a function of the horizontal

distance: x, v_y and v_x are the vertical and horizontal components of the material velocity vector of the surface, v_{sedim} and $v_{erosion}$ are the sedimentation and erosion rates, respectively (Gerya and Yuen, 2007; Gorczyk et al., 2007). Building on previous similar models (Gorczyk et al. 2007; Vogt et al. 2012) we show model results where partial melting is also considered (Modmelt in Table 2). Following these previous models, it is assumed that the degree of both hydrous and dry melting is a function of pressure and temperature (e.g., Gerya and Yuen, 2007) and melt ascend is simulated by extracting all melt exceeding locally, a pre-defined melt extraction threshold. Extracted melts are transmitted instantaneously to emplacement areas in form of plutons and volcanics. It is assumed that 20% of all extracted melts propagate towards the surface forming a volcanic arc above the extraction area, whereas remaining melts intrude into the middle-lower crust under the arc (Vogt et al. 2012). A more detailed description of the numerical approach is available in Gerya (2010) and in the supplementary material.

Numerical models	Ocean length	Sedimentation rate	Upper plate WZ	Boundary condition	Boundary condition duration
Modref	km	km/Myr	Hydrated mantle	V_l=1.5 cm/yr	Entire model run
Modhot	km	km/Myr	Hydrated mantle and higher T_{moho}	V_l=1.5 cm/yr	Entire model run
Modlong	km	km/Myr	Hydrated mantle	V_l=1.5 cm/yr	Entire model run
Modcr	km	km/Myr	Hydrated mantle and crustal WZ	V_l=1.5 cm/yr	Entire model run
Modhom	km	km/Myr	none	V_l=1.5 cm/yr	Entire model run
Modhomlong		km/Myr	none	V_l=1.5 cm/yr	Entire model run
Modmelt	km	km/Myr	Volcanic arc	V_l=1.5 cm/yr	Entire model run
Modfre	km	km/Myr	Hydrated mantle	V_l=1.5 cm/yr	Until 36 Myr
Modtw	km	km/Myr	Hydrated mantle	V_l=V_u=0.75 cm/yr	Entire model run
Modtwfr	km	km/Myr	Hydrated mantle	V_l=V_u=0.75 cm/yr	Until 36 Myr

Numerical models	Ocean length	Sedimentation rate	Upper plate WZ	Boundary condition	Boundary condition duration
Modwzrev	km	km/Myr	Hydrated mantle	V_l=1.5 cm/yr	Entire model run
Modlosed	km	km/Myr	none	V_l=1.5 cm/yr	Entire model run
Modhised	km	km/Myr	none	V_l=1.5 cm/yr	Entire model run
Modlosedfr	km	km/Myr	none	V_l=1.5 cm/yr	Until 30 Myr
Modhisedfr	km	km/Myr	none	V_l=1.5 cm/yr	Until 30 Myr

Table 2. 2D model parameter tests. In a visco-plastic experiment (Modmelt) melt extraction is implemented and the development of a volcanic arc is simulated. Further model results are shown in the supplementary material file.

2.2 Model setup

The models simulate horizontally forced subduction of an oceanic plate beneath a continental margin on a lithospheric to upper mantle cross-section sized 4000 × 720 km^2. The rectangular grid of 1361 × 283 nodal points is non-uniform and contains a 1000 km wide high-resolution area of 1 × 1 km^2 in the center of the domain that gradually changes to 10 × 10 km^2 towards the model sides (Fig. 2). The downgoing plate is built up by an oceanic and continental lithosphere connected by a 150 km wide passive margin. The width of the oceanic domain is varied between 550 km and 1000 km. The continental crust consists of 20 km upper crust (wet quartzite rheology) and further 15 km lower crust (plagioclase rheology). The overriding continent also hosts a 275 km wide orogenic area of increased upper and lower crustal thickness of 21 km and 18 km, respectively. Furthermore, underneath this orogenic segment an inclined weak zone of wet olivine rheology is defined in the lithospheric mantle, representing an inherited suture zone (Fig. 3). The role of different upper plate weak zones is assessed in a parameter test (Fig. 4). The oceanic crust is represented by 3 km basalt and further 5 km gabbroic crust. Both the lithospheric and the sub-lithospheric mantle are composed of anhydrous peridotite (dry olivine rheology). An inclined weak zone defined by low plastic strength and wet olivine rheology is placed along the active margin to initiate subduction (Fig. 2).

Free slip boundary condition is defined on all model sides. 20 km sticky air is defined on top of the model to simulate an internal free erosion/sedimentation surface (cf., Crameri et al., 2012). Sedimentation rate is varied in a series of experiments between 0-0.5 km/Myr. In order to initiate subduction, a horizontal velocity condition of 1.5 cm/yr is defined on the lower plate or on both plates. This boundary condition is kept constant in a series of models or turned off

in another series of experiments after the slab reaches ca. 350 km depth. In another series of experiments the velocity boundary condition is set to 0 during continental collision stage. The initial thermal properties of the left and right continents are horizontally uniform reaching 0 °C on the surface, 645 °C at Moho depth and 1300 °C at 110 km depth representing the base of the lithosphere. The thermal structure of the ocean is defined using a half-space cooling model with uniform oceanic plate age of 50 Myr. The asthenospheric mantle is characterized by an initial adiabatic temperature gradient of 0.5 °C /km. Our applied rheological and thermal values are similar to values from geological reconstructions of the Mediterranean region prior to back-arc extension (Faccenna et al., 2014). Further models analyzing the influence of different rheological layering and initial temperature profiles are shown in the supporting information file.

1. **Results**

All our models evolve in four distinct stages associated with specific tectonic processes and mantle flow patterns. *Stage 1: forced subduction initiation* along a former passive margin governed by far-field compression (e.g., Toth and Gurnis, 1998; Faccenna et al., 1999) leading to the initial underthrusting of the oceanic plate beneath the continental margin and associated upper crustal deformation. *Stage 2: mature oceanic subduction* showing the gradual consumption of the oceanic lithosphere, slab steepening and gradually increasing mantle return flow velocity. *Stage 3: soft collision and onset of continental subduction* marking the subduction of the extended continental passive margin of the lower plate. *Stage 4: hard collision* is associated with the arrival of the unextended continental lithosphere into the subduction zone leading to upper crustal exhumation and orogenic build-up preceding slab break-off. All the models show the evolution of a forearc topographic high and a topographic depression in the upper plate overlying the subduction interface and the mantle wedge. Furthermore, surface subsidence is also simulated at larger distances from the subduction zone controlled by crustal thinning. In the following we classify the topographic depression above the subduction interface to be a retro-forearc basin and the more distal depression as a back-arc basin.

Every model simulates the subduction of the hydrated oceanic crust and sediments into the upper mantle where dehydration takes place. Fluids are released from the slab and hydrates the subduction interface and the overlying lithosphere, while the influence of melts and the formation of a volcanic arc is simulated in certain experiments.

3.1 Reference model

The reference model includes the narrower, i.e., 550 km oceanic basin and constant velocity condition imposed on the lower plate, while the upper plate is fixed. A hydrated weak zone is placed at 400 km horizontal distance from the active margin within the mantle (Fig. 3). During stage 1 subduction initiation and the first 17 Myr of convergence show slow trench advance and compressional stress accumulation in the upper plate. Sediments are deposited in the ca. 7 km

deep trench forming an accretionary wedge. A pronounced forearc high and a topographic depression is formed in the upper plate showing a forearc syncline structure. The depocenter of this syncline is located at ca. 200 km distance from the accretionary wedge. It subsides ca. 1 km during the first 10 Myr that is followed by additional 1 km subsidence until 20 Myr. The area above the distal mantle weak zone is uplifted due to contractional strain localization and further crustal thickening (Fig. 3a-b).

Trench advance is switched to trench retreat during stage 2 (Figs. 3c,d). The mantle return flow velocity gradually increases, the accretionary wedge is thickening. Both the upper and lower plate records extensional stress field. Trench retreat also results in a decreasing slab dip angle. The syncline structure of the forearc basin in the upper plate records slow, ca. 30 m/Myr uplift from 35 Myr. Besides the uplift of the retro-forearc basin, the continental upper plate gets tilted towards the trench, leading to the subsidence of the former forearc high and resulting in a trenchward shift of the main depocenter location between the accretionary wedge and the former forearc syncline. Furthermore, slab retreat is accommodated by upper plate extension. First, the previously thickened crustal area undergoes negative tectonic inversion associated with ca. 100 m/Myr subsidence rate that is followed by distributed normal faulting over a larger area with lower, ca. 25-50 m/Myr subsidence rate. Finally, localized rifting takes place with up to 225 m/Myr subsidence rate in a distal continental back-arc basin (Figs. 3c,d).

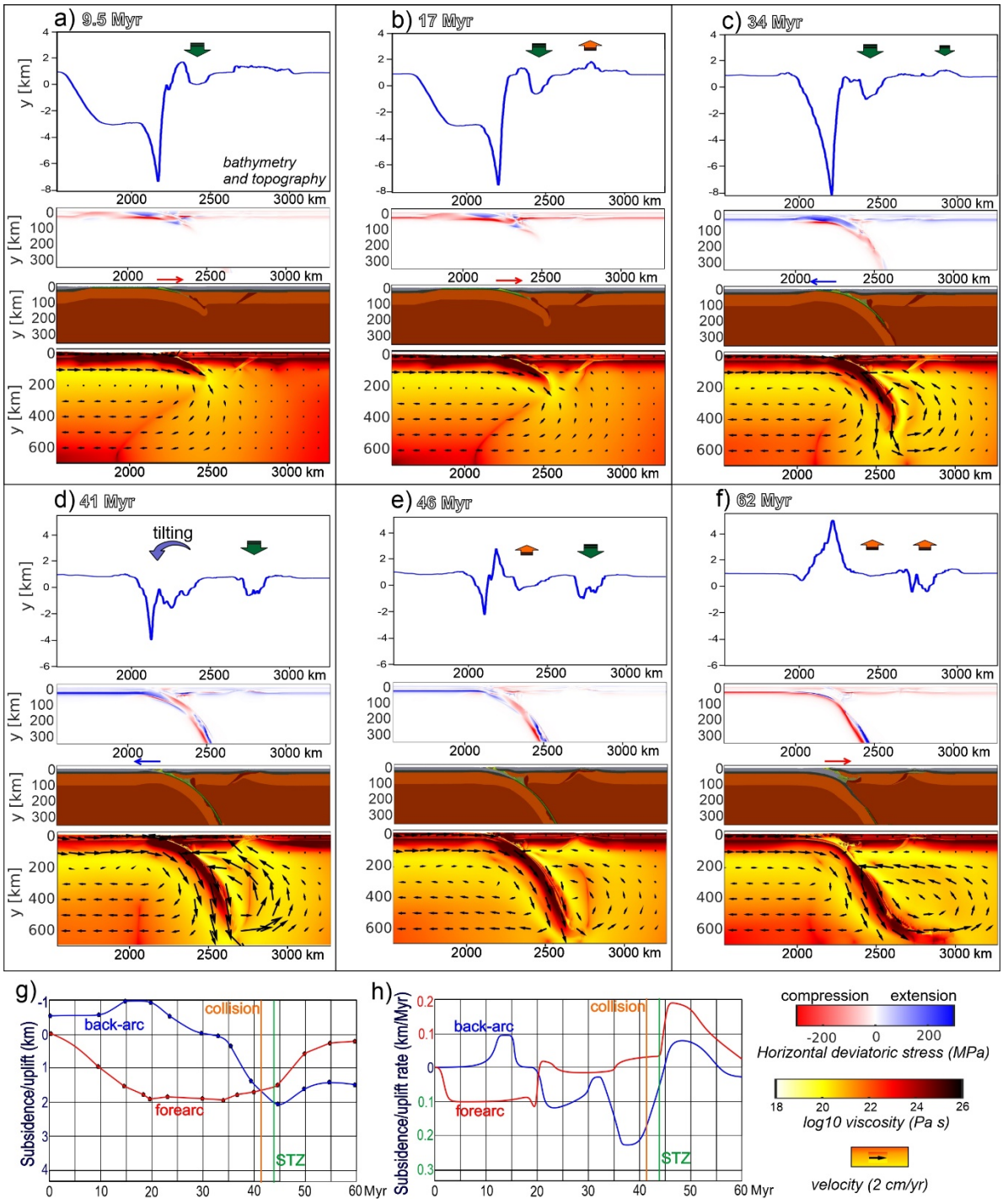
a) 9.5 Myr
b) 17 Myr
c) 34 Myr
d) 41 Myr
e) 46 Myr
f) 62 Myr
bathymetry and topography
tilting
y [km]
2000
2500
3000 km
g)
h)
Subsidence/uplift (km)
Subsidence/uplift rate (km/Myr)
back-arc
forearc
collision
STZ
60 Myr
compression
extension
-200
0
200
Horizontal deviatoric stress (MPa)
18
20
22
24
26
log10 viscosity (Pa s)
velocity (2 cm/yr)

Figure 3. a-f) Evolution of the reference model (Modref) showing effective viscosity sections overlain by velocity vectors, rock composition, horizontal deviatoric stress ($_{xx}$) results and topography. Green and red arrows over the topography plots indicate subsidence and uplift, respectively. Blue and red arrows over the rock composition figures indicate trench retreat and advance, respectively. g) Long-term subsidence history of the forearc and back-arc regions. h) Long-term vertical motion rates of the forearc and back-arc regions. STZ – onset of slab transition zone interaction.

Stage 3 and soft collision starts from 41 Myr (Figs. 3d,e). All the trench, the previously tilted upper plate continental and the former retro-forearc basin are rapidly uplifted, the accretionary wedge is also thrusted above sea-level due to the convergence of the lower and upper continental plates (Fig. 3d). By 43 Myr the leading edge of the slab reaches the 660 km lower boundary. Forearc basin uplift is accelerated to ca. 200 m/Myr rate, while the slab is still retreating during the subduction of the extended continental passive margin until 46 Myr, controlling continuous back-arc lithospheric thinning and subsidence (Fig. 3e). Finally, during stage 4 of hard collision, a high orogen is formed upon the ongoing slow convergence. The upper crust is decoupled and detaches from the lower crust of the downgoing plate and it is accreted into the orogen. Both the upper and lower plates record compression at this time leading to positive basin inversion and uplift of the previously formed intra-continental back-arc basin in the upper plate (Fig. 3f). Slab necking is observed from 62 Myr preceding slab break-off.

3.2 Sensitivity analysis

We test the sensitivity of the reference model by varying its initial configuration, by applying different kinematic conditions and by modifying its rheology, including the presence of weak zones in the upper plate, the role of melting and the influence of different volumes of sediment subduction.

3.2.1 The role of different oceanic basin length

Designing an almost two times longer, 1000 km wide oceanic lower plate allows the development of greater slab-pull due to a long-lasting oceanic subduction stage prior to continental collision. Furthermore, in the reference model the leading edge of the slab reached the bottom of the upper mantle at the onset of collision, while in the model with a longer ocean (Modlong, Fig. 4) these two events are diachronous and thus their distinct effects can be assessed. All other parameters are kept the same as in the reference model including a hydrated mantle weak zone in the upper plate.

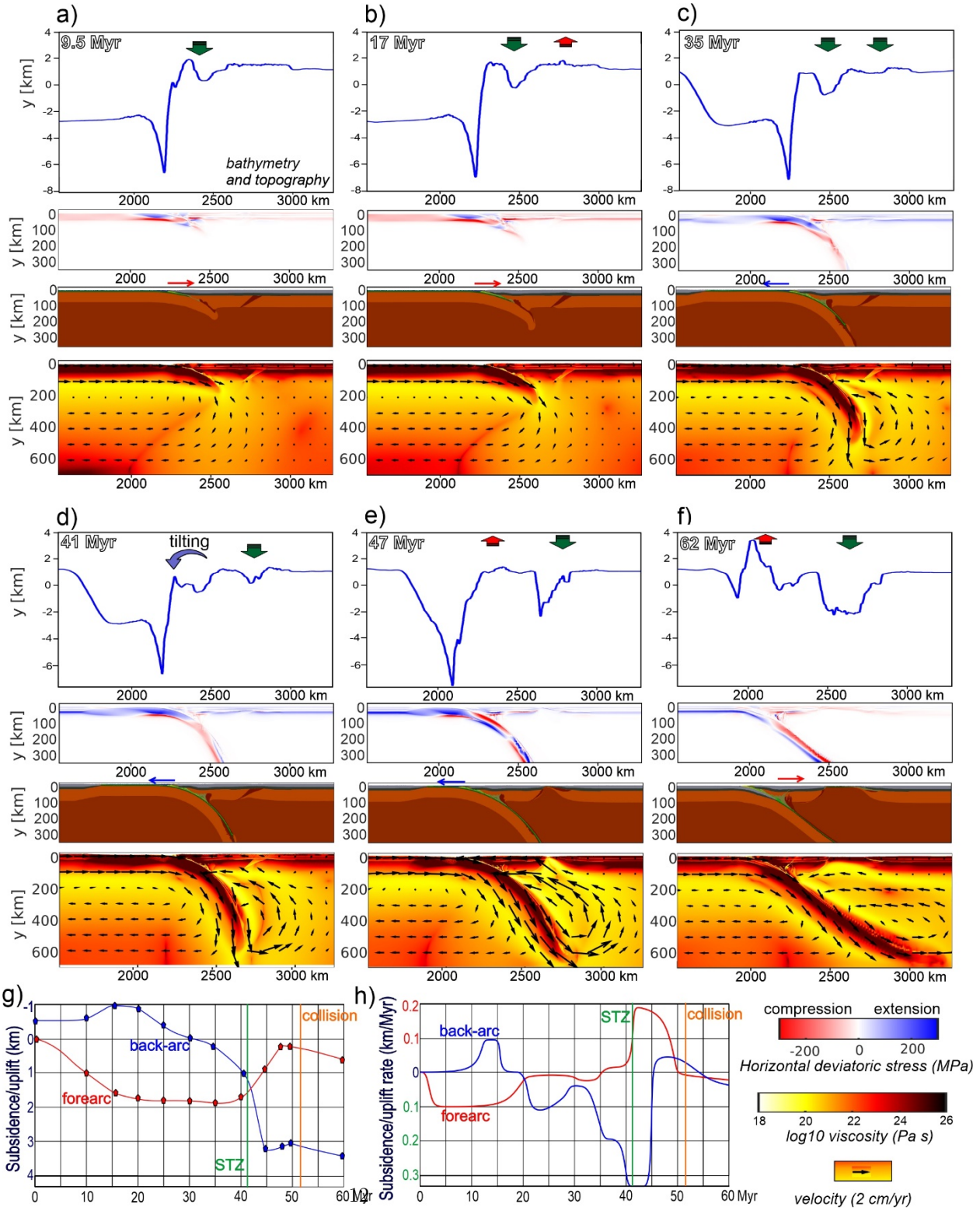
a)
9.5 Myr
bathymetry
and topography
b)
17 Myr
c)
35 Myr
d)
41 Myr
tilting
e)
47 Myr
f)
62 Myr
y [km]
2000
2500
3000 km
g)
Subsidence/uplift (km)
back-arc
forearc
STZ
collision
60 Myr
h)
Subsidence/uplift rate (km/Myr)
compression
extension
-200
0
200
Horizontal deviatoric stress (MPa)
18
20
22
24
26
log10 viscosity (Pa s)
velocity (2 cm/yr)

Figure 4. a-f) Evolution of the model including a longer oceanic lower plate (Modlong) showing effective viscosity sections overlain by velocity vectors, rock composition, horizontal deviatoric stress ($_{xx}$) results and topography. Green and red arrows over the topography plots indicate subsidence and uplift, respectively. Blue and red arrows over the rock composition figures indicate trench retreat and advance, respectively. g) Long-term subsidence history of the forearc and back-arc regions. h) Long-term vertical motion rates of the forearc and back-arc regions. STZ – onset of slab transition zone interaction.

Stages 1 and 2 are similar in Modref (Figs. 3a-c) and Modlong (Figs. 4a-c), but the longer oceanic subduction enables higher trench retreat and thus higher upper plate extension values leading to crustal break-up after the distal back-arc rifting stage (Figs. 4 d,e). Like in the reference model, the upper plate records trench-ward tilting leading to slow uplift of the retro-forearc basin from the onset of trench retreat (Fig. 4d). When the leading edge of the slab reaches the 660 km model boundary the forearc uplift rate increases to 0.2 km/Myr, while subsidence of the back-arc basin reaches a maximum of 0.35 km/Myr during the rapid slab roll-back and back-arc lithospheric stretching (Fig. 4e). This is a relevant surface signal in the system reflecting deep subduction dynamics. During soft collision from 50 Myr, the trench records ongoing retreat and the back-arc oceanic spreading continues until hard collision. From ca. 60 Myr trench advance leads to upper plate compression and incipient subduction initiation of the former back-arc ocean (Fig. 4f, Fig. S1).

3.2.2 The role of subduction and convergence kinematics

We evaluate the influence of upper plate and lower plate velocity conditions and their temporal variations on forearc and back-arc basin evolution (Fig. 5). When the convergence velocity of 1.5 cm/yr is equally partitioned between the lower and upper plate (Modtwfr) the slab dip angle is expectedly lower (e.g., van Hunen et al., 2000, 2004) and the subduction curvature radius is larger compared to the model where only the lower plate was pushed (Modfre). In the latter model of a more shallow-dipping subduction, the forearc basin subsidence is ca. 320 m lower than in the reference model (cf., Figs. 5 a,d). Furthermore, the upper plate is affected by larger extensional stresses and back-arc extensional deformation in the reference model, while in the model with both upper and lower plate convergence velocities slab roll-back is mainly accommodated by the imposed upper plate velocity and suppressed back-arc intraplate deformation is observed (cf. Figs. 5 a,d).

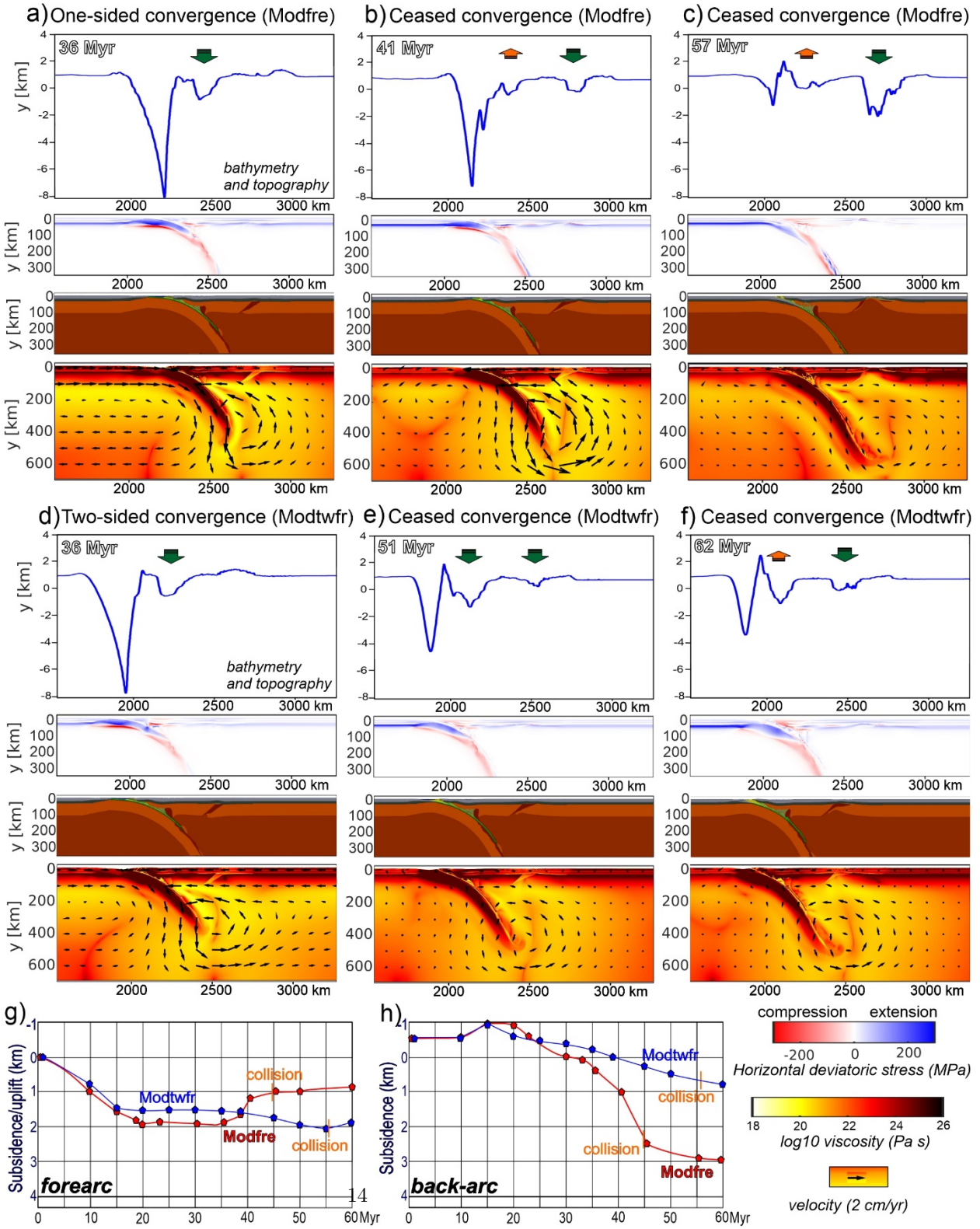
a) One-sided convergence (Modfre)
b) Ceased convergence (Modfre)
c) Ceased convergence (Modfre)
d) Two-sided convergence (Modtwfr)
e) Ceased convergence (Modtwfr)
f) Ceased convergence (Modtwfr)
36 Myr
41 Myr
57 Myr
51 Myr
62 Myr
bathymetry and topography
y [km]
2000
2500
3000 km
g)
h)
Subsidence/uplift (km)
Subsidence (km)
Modtwfr
Modfre
collision
forearc
back-arc
0
10
20
30
40
50
60 Myr
compression
extension
-200
0
200
Horizontal deviatoric stress (MPa)
18
20
22
24
26
log10 viscosity (Pa s)
velocity (2 cm/yr)

Figure 5. Parameter test on the influence of variable convergence velocities. (a) Convergence velocity is applied only on the lower plate. (b-c) No velocity boundary conditions are imposed. Subduction is accommodated by upper plate extension. (d) Convergence velocity is applied on both the lower and upper plates. (e-f) No velocity boundary conditions are imposed. Subduction is accommodated by upper plate extension. g-h) Long-term subsidence history of the forearc and back-arc regions.

The convergence velocities are set to 0 after 36 Myr in both models representing fixed upper and lower plates. From this stage the slabs show continuous roll-back that is solely accommodated by upper plate extension. Note that by this stage the two models record the same convergence value, however, the amount of subduction is larger in the model where the upper plate was initially fixed (Modfre) and this created larger values of slab roll-back and trench retreat. The leading edge of the slab in model Modfre is at 450 km depth, while in Modtwfr this depth is only 380 km by 36 Myr (Figs. 5a,d). The shallower dipping slab in Modtwfr undergoes steepening during the ceased convergence phase. Free-fall subduction results in slab roll-back and upper plate extension in both models. Modfre shows a similar topographic evolution like the reference model, although larger slab retreat is recorded leading to larger upper plate extension values. The maximum slab roll-back and trench retreat velocity is 1.8 cm/yr at 40 Myr. The forearc basin also shows slow uplift rate from 36 Myr and the upper plate is tilted towards the trench until soft collision and the arrival of the slab to the model bottom leading to rapid forearc uplift (Figs. 5b,c). The model where the initial convergence was imposed on both the upper and lower plates and the slab was initially more shallow-dipping, shows smaller slab roll-back rates and overall lower mantle flow velocity (Fig. 5e). These values gradually increase to a maximum of 1.2 cm/yr until soft collision is recorded (Fig. 5f). In this model gradual slab steepening continues and the forearc basin shows gradual slow subsidence until soft collision, reaching a maximum forearc basement depth of 2500 meters at 51 Myr.

3.2.3 The role of upper plate strength

We present the influence of a weaker upper plate where an additional crustal weak zone is placed above the hydrated mantle and all other parameters are kept identical to the reference model with a shorter oceanic lower plate (Modcr in Fig. 6a). This model evolution is compared with two other models having strong and homogeneous upper plates including a shorter oceanic (Modhom in Fig. 6b) and a longer oceanic basin (Modhomlong in Fig. 6c).

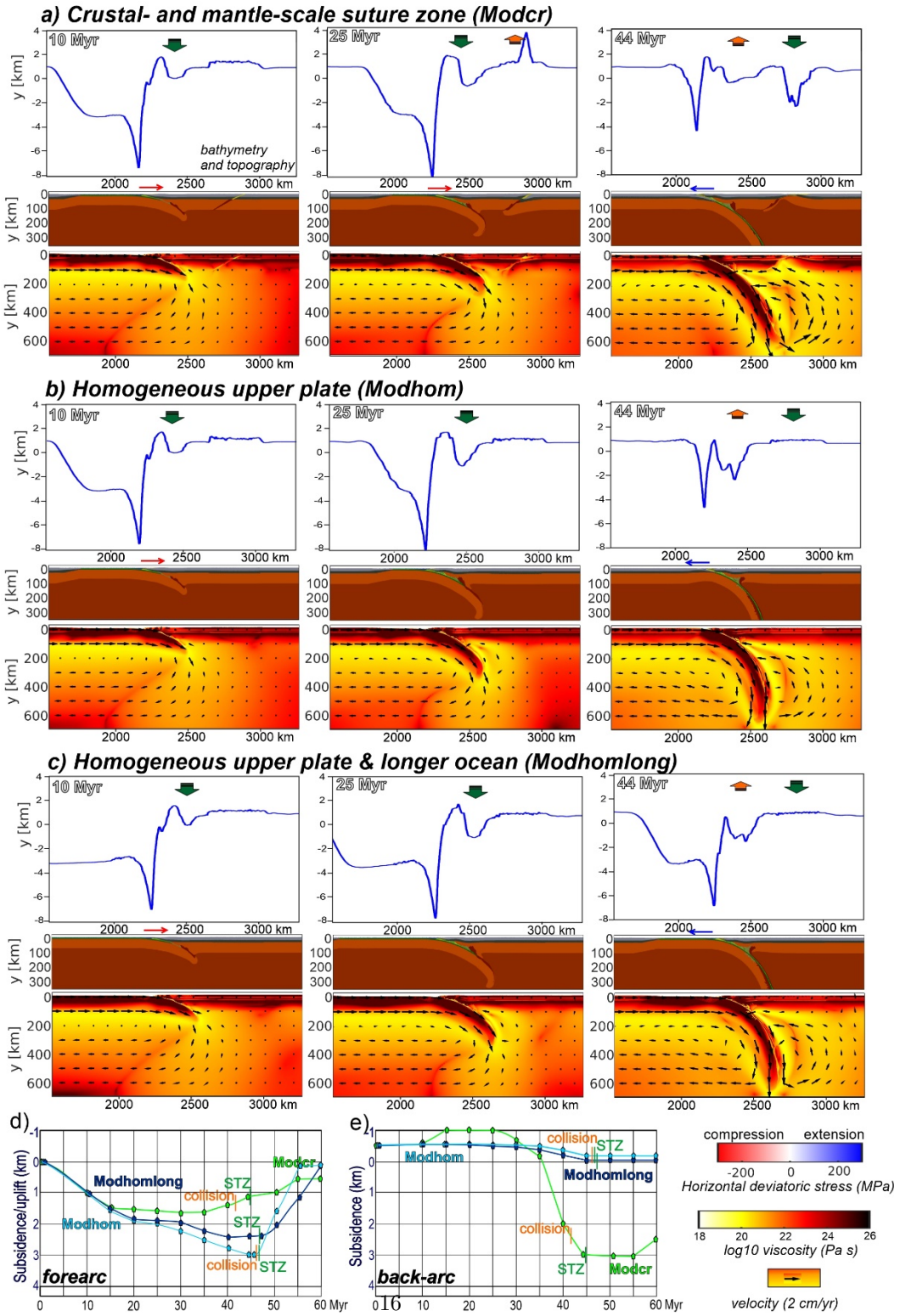
a) Crustal- and mantle-scale suture zone (Modcr)
b) Homogeneous upper plate (Modhom)
c) Homogeneous upper plate & longer ocean (Modhomlong)
10 Myr
25 Myr
44 Myr
bathymetry
and topography
y [km]
2000
2500
3000 km
d)
e)
Subsidence/uplift (km)
Subsidence (km)
Modhomlong
Modhom
Modcr
STZ
collision
forearc
back-arc
0
10
20
30
40
50
60 Myr
compression
extension
-200
0
200
Horizontal deviatoric stress (MPa)
18
20
22
24
26
log10 viscosity (Pa s)
velocity (2 cm/yr)

Figure 6. Parameter test on the influence of a longer oceanic basin and different upper plate rheological heterogeneities shown by effective viscosity sections overlain by velocity vectors, rock composition results and topography. STZ – onset of slab transition zone interaction. d-e) Long-term subsidence history of the forearc and back-arc regions.

In the model where both crustal and mantle weak zones are present (Fig. 6a) the magnitude of initial trench advance that is accommodated by upper plate shortening, is ca. 90 km, while this magnitude is only 50 km in the reference model and only ca. 40 km in Modhom and Modhomlong. In Modcr contractional strain is localized along the continuous inherited lithospheric-scale structure leading to the inception of continental subduction, while in Modref and Modlong including the mantle weak zone, shortening was accommodated by a series of thrusts distributed above the weak zone. In the model having the weakest upper plate (Modcr) trench advance and compression also lasts longer than in the reference model (Fig. 10). During stage 2 every model show the subsequent extensional reactivation of the previously compressed zone driven by slab roll-back and trench retreat. Modref and Modlong show the migration of extensional structures in the crust from the initial location of the weak zone towards its dip direction, while the inherited hydrated weak zone is gradually re-distributed at the base of the crust (Figs. 3, 4). In the model with both crustal and mantle weak zones (Modcr) extension reactivates the inherited shear zone leading to a narrower structure, an earlier crustal break-up and lithospheric mantle exhumation within the back-arc region (Fig. 6a). In the strong models trench retreat is suppressed reaching only ca. 20-30 km.

The greatest forearc subsidence value is observed in the models with a strong homogenous upper plate reaching 2.3 km and 3 km in Modhomlong and Modhom, respectively, while the lowest forearc subsidence is simulated in the weakest model (Modcr) having both crustal and mantle weak zones (Fig. 6). In this model the highest back-arc subsidence rate is observed from 35 Myr. In all these models, subsidence of the forearc region terminates during slab roll-back and upper plate extension that controls back-arc subsidence. The highest forearc subsidence rate is always observed after the leading edge of the slab reaches the lower model boundary (Fig. 6d).

3.2.4 The role of melt extraction

A model is shown analyzing the influence of melt extraction and related weakening effects (Fig. 7). This model also assumes more simple visco-plastic rheology that does not involve elasticity. The early stages of model evolution are similar to the reference model showing the gradual subsidence of a retro-forearc basin, an initial stage of upper plate compression and subsequent slab retreat and upper plate extension. The initial forearc subsidence is lower than in the reference model, it reaches 0.5 km until 10 Myr and 1.8 km by 25 Myr. The depocenter is located at the same ca. 250 km distance from the accretionary wedge as in the reference model, while in this experiment a volcanic arc evolves initially at ca. 280 km from the accretionary wedge (Fig. 7b). The volcanic arc is ini-

tially fed by melt extraction from partially molten subducted (meta)basalt and hydrated peridotites formed atop the slab by fluid-fluxed melting. Similarly to the reference model, the mantle return flow velocity increases with the gradually increasing slab depth, and the slab starts to roll-back (Fig. 7c). Slab roll-back and trench retreat are accommodated by upper plate extension, noticeable deformation is initially distributed in the thickened crust like the model without a weak zone. Slab retreat is accelerated from 27 Myr leading to the rapid ascent of the asthenosphere. Extension is ultimately localized along the active volcanic arc, weakened by extracted melts (Vogt et al., 2012) leading to arc rifting and rapid break-up of the lithosphere at ca. 130 km distance from the oldest volcanic arc region mirroring the same amount of slab retreat by this time (Fig. 7c). Slab roll-back and the mantle flow velocity rapidly increases from rifting to break-up. Lithospheric mantle thinning is linked to decompressional melting leading to the formation of a new oceanic basin in between the oldest and active volcanic arcs (Figs. 7c-d). The latter is sourced by both asthenospheric decompressional melts and by molten subducted basalts, sediments and peridotites through the hydrated mantle wedge. By 30 Myr the slab breaks-off at ca. 100 km depth leading to the rapid uplift of the overlying area as well as emplacement of volcanic rocks above the descending slab (Fig. 7d). The previously formed forearc basin and sediments are drifted away by the newly formed ocean. The final snapshot of the model shows an orogenic suture and the uplifted remnants of the former forearc sediments separated by a wide oceanic basin (Fig. 7e).

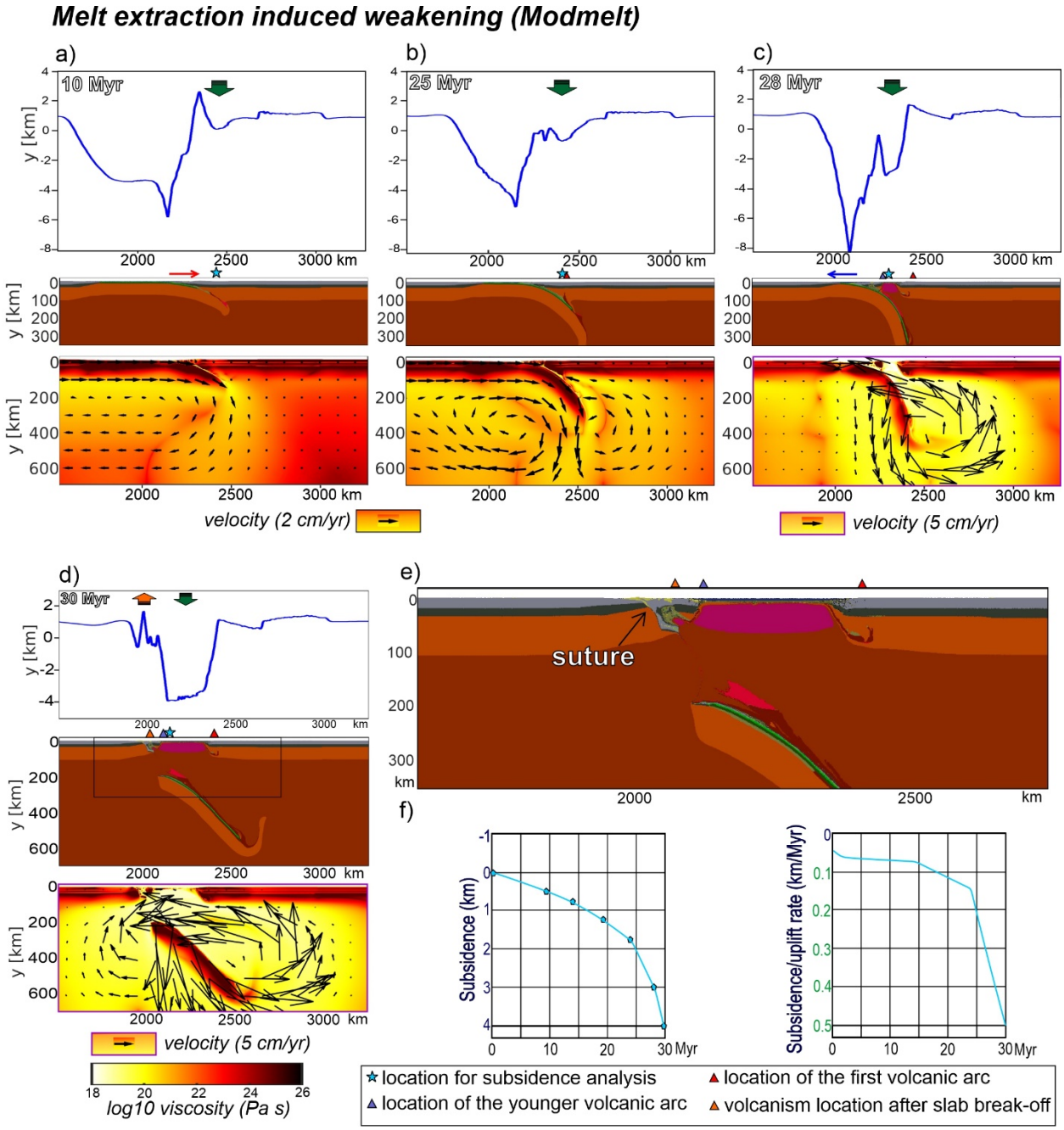

Figure 7. Role of melt extraction on forearc and back-arc basin evolution shown by effective viscosity sections overlain by velocity vectors, rock composition results and topography. Red and Blue triangles indicate the location of an older

and younger volcanic arc region, respectively. Orange triangle indicates the location of volcanism after slab break-off. f) Long-term subsidence history and subsidence rates of the forearc depocenter that evolves into a back-arc basin after arc rifting.

3.2.5 The role of erosion and sedimentation

The influence of different erosion and sedimentation rates is assessed by four further simulations, where the upper plate is fixed and is kept homogenous, and the longer oceanic basin is used in order to isolate the surface processes control from any other effects. In two models (Modlosed and Modhised) constant 1.5 cm/yr velocity is imposed on the lower plate throughout the entire model run (Fig. 8). Stage 1 of incipient subduction is similar in the models with lower and higher sedimentation rates, compressional stress is accumulated in the upper plate, the retro-forearc basin records ca. 1.75 km subsidence. After 36 Myr of subduction a much thicker accretionary wedge developed in the subduction zone, furthermore the subducted sediments are underplated below the forearc high and are further subducted within the subduction interface having notably greater thickness (Fig. 8). The retro-forearc basin subsidence in the models with lower and higher sedimentation rate is 2.4 km and 1.8 km, respectively. The model with higher sedimentation rate also shows a more shallow-dipping subduction zone compared to the model with lower sedimentation rate (Fig. 8). Furthermore, the accumulated extensional stress in the upper plate reached ca. 200 MPa in the model with lower sedimentation, while this value is only 110 MPa in the models with higher sedimentation.

In two further models with lower and higher erosion rates the boundary velocity condition is turned off after 30 Myr when the leading edge of the slab is at ca. 380 km depth (Fig. 9). Thereafter subduction velocity is solely determined by the dynamics and forces within the system. In the model with higher sedimentation rates subduction velocity is first dropped down to 1.2 cm/yr and then gradually increases to 4.8 cm/yr by 46 Myr before the slab reaches the bottom of the model. In the model with lower sedimentation rate the subduction velocity gradually increases from the initially pre-defined 1.5 cm/yr to 2.6 cm/yr by 33 Myr and reaches a maximum of 7.1 cm/yr by 35 Myr during free-fall subduction (Fig. 9). Similarly to the previous two models (Figs., 8-9), the higher sedimentation rate implies lower retro-forearc subsidence reaching 1.85 km depth and lower extensional stress accumulation of 125 MPa. The forearc basin subsides to 2.25 by 33 Myr with lower erosion rates. During the high velocity free-fall subduction stage a larger dynamic subsidence is observed reaching a maximum of 3.2 km before the slab reached the bottom of the model (Fig. 9).

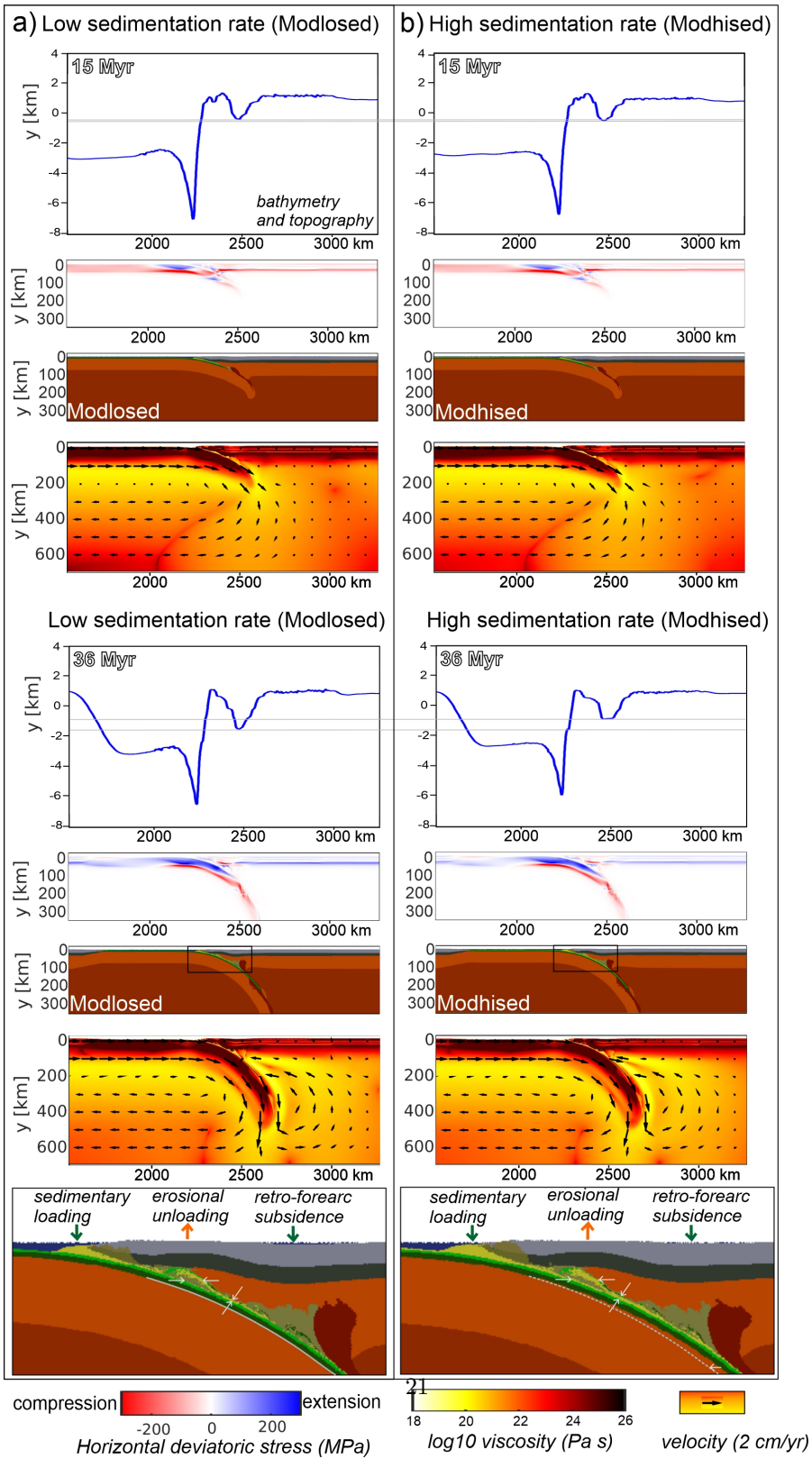
a) Low sedimentation rate (Modlosed)
b) High sedimentation rate (Modhised)
15 Myr
bathymetry and topography
y [km]
2000
2500
3000 km
Modlosed
Modhised
Low sedimentation rate (Modlosed)
High sedimentation rate (Modhised)
36 Myr
sedimentary loading
erosional unloading
retro-forearc subsidence
compression
extension
-200
0
200
Horizontal deviatoric stress (MPa)
18
20
22
24
26
log10 viscosity (Pa s)
velocity (2 cm/yr)

Figure 8. Parameter test on the influence of different erosion and sedimentation rates. Constant velocity condition is imposed on the lower plate. Note that thicker sediment accumulation results in a weaker subduction interface and less efficient stress transfer towards the upper plate and lower forearc basin subsidence. Furthermore, higher erosion and sedimentation rates lead to a shallower dipping slab. Dashed white line in the compositional figure with higher sedimentation rate shows the slab geometry of Modlosed.

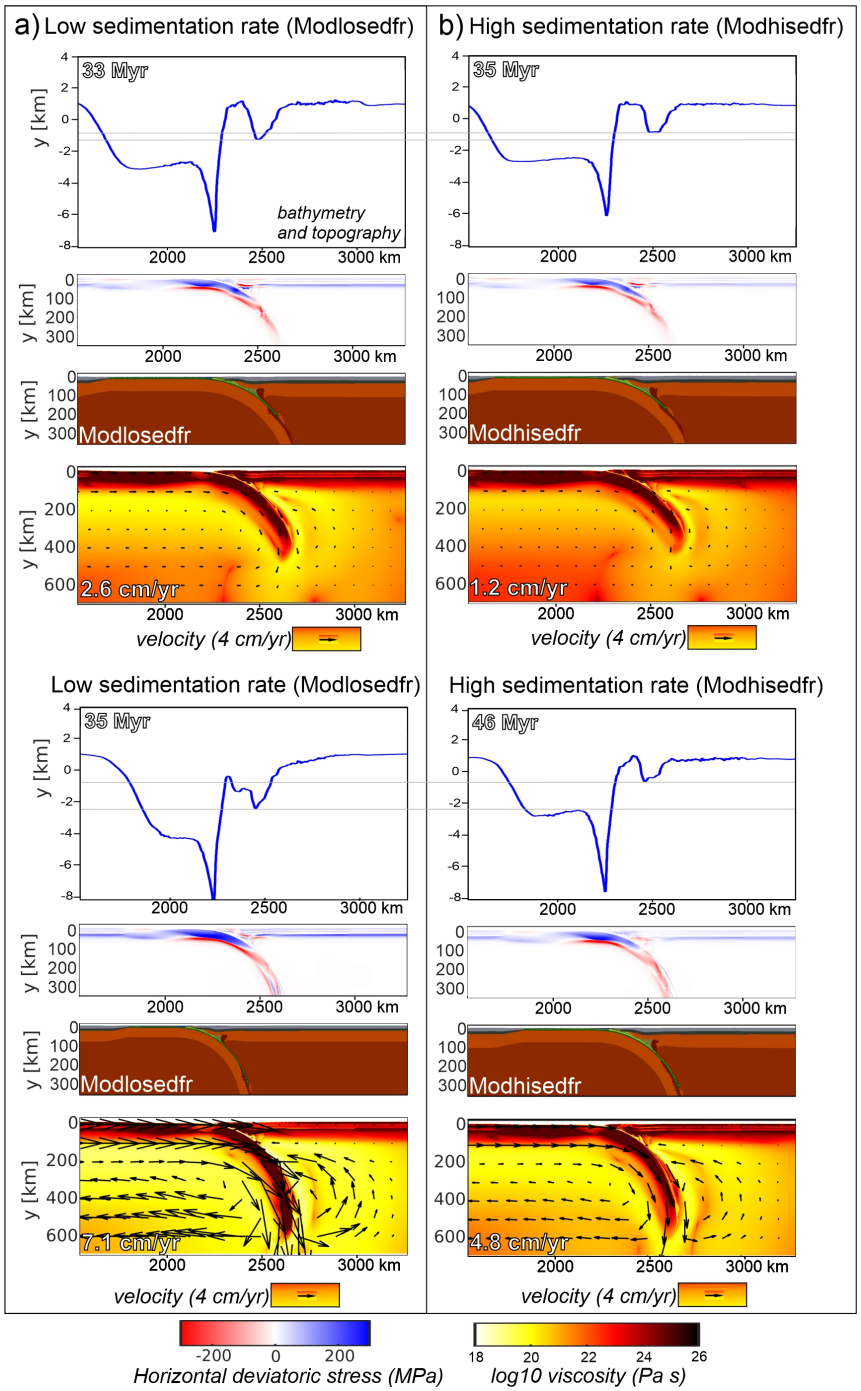

Figure 9. Parameter test on the influence of different erosion and sedimen-

tation rates. No velocity boundary conditions are imposed. Note that higher subduction velocity is reached in the experiment with lower sedimentation and erosion rates.

1. Discussion

(a) Slab dynamics versus stress field and surface processes

Our models show common evolution in terms of trench and S-point kinematics (Fig. 10). Horizontally forced subduction initiation stage is associated with trench advance and upper plate compression. The resulted contraction is partitioned between the forearc region leading to the development of a forearc high and a compressional retro-forearc depression and in case of additional upper plate weak zones contraction also reactivates the crustal or mantle weak zone in the back-arc region (Figs. 3-6). Mature oceanic subduction is linked to slab roll-back and trench retreat. The maximum trench retreat velocity varies in the different models between 2.5-7.5 cm/yr (Fig. 10) and it is accommodated by upper plate extension. In the models where melt extraction and arc rifting were simulated, and the resulted mantle viscosity is the lowest, the highest 7.5 cm/yr trench retreat velocity is achieved prior to continental subduction and slab break-off (Fig. 7). In the models where melt extraction is not simulated, but a weak zone is defined in the upper plate, a longer lithospheric thinning phase is modeled, and the trench retreat velocity gradually increases until the arrival of the buoyant continental material into the subduction zone (Fig. 10). These 2D models, in agreement with previous similar studies (e.g., Magni et al., 2012) imply that the trench retreat velocity is mainly controlled by the gradually increasing slab-pull force together with the increasing mantle return flow velocity that fosters slab roll-back. Furthermore, notable trench retreat is only observed in the models where the upper plate is weakened, either above the simulated hydrated mantle wedge within the volcanic arc or due to inherited weak zones (cf., Yang et al., 2021). Some previous studies also inferred the role of viscous drag along the base of the upper plate that can contribute to back-arc extensional stresses, particularly for large plates and higher asthenospheric viscosities (e.g., Capitanio et al., 2010; Dal Zilio et al., 2018).

Trench advance and subsequent retreat reached the highest values in the model where both crustal and mantle weak zones were defined (Fig. 6) and thus the upper plate had the lowest strength (Fig. 6), while in the model where the upper plate contained no weak zone, trench movements remained suppressed. Furthermore, trench retreat and upper plate extension velocity gradually increases as the strength of the upper plate is decreasing during rifting leading to accelerated rift and plate velocities (cf., Brune et al., 2016). Following continental hard collision and the subduction of the buoyant continental crust, trench retreat switches to trench advance and results in upper plate compression prior to slab break-off.

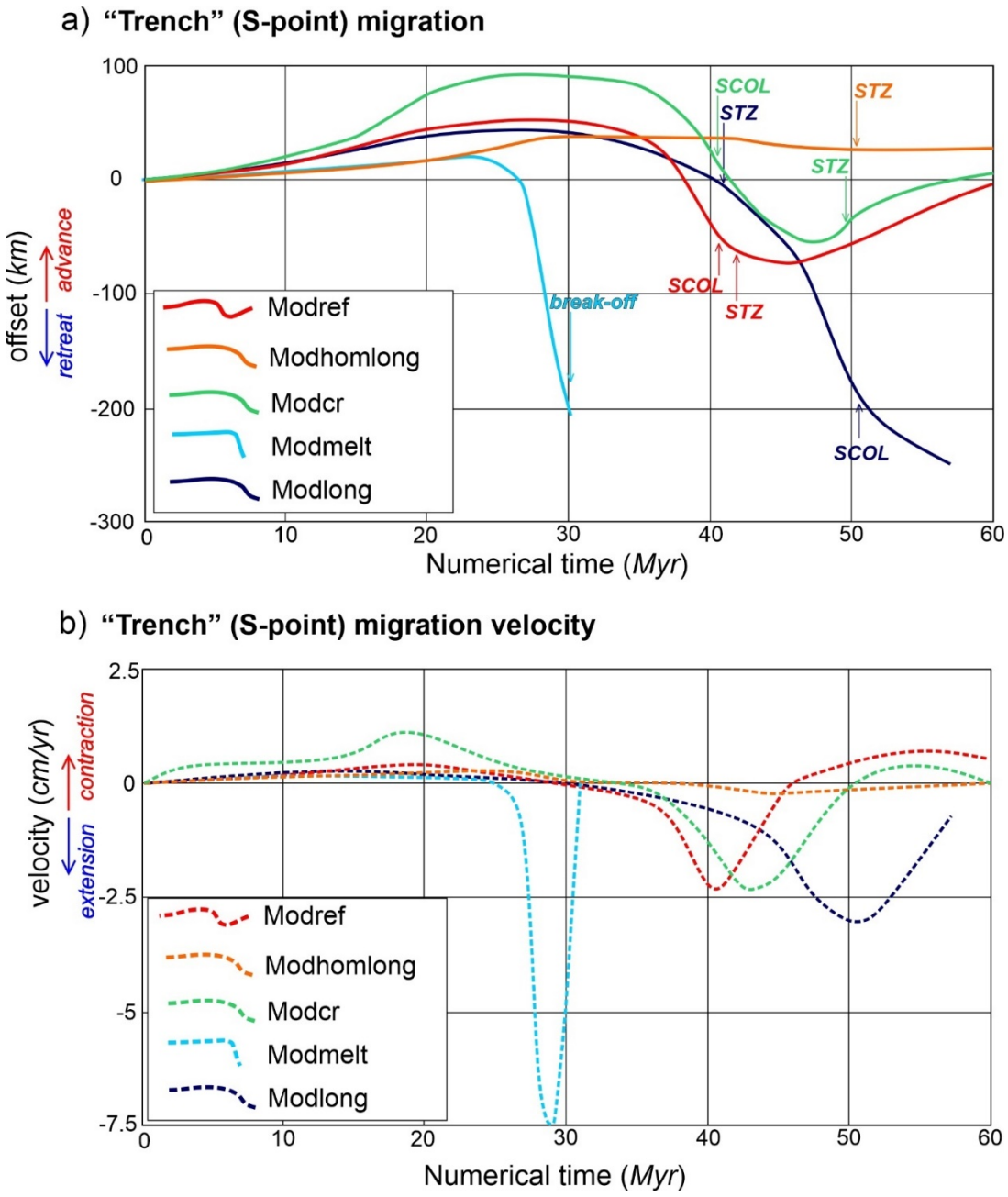

Figure 10. Slab dynamics during oceanic and continental subduction shown by the lateral position and velocity of the singularity point. STZ – slab transition zone interaction, SCOL – soft collision.

Stress transfer from the trench towards the upper plate is controlled by the

strength and viscosity of the subduction interface (e.g., Buiter et al., 2001; Billen and Gurnis, 2001; Cizkova and Bina, 2013; Cerpa and Arcay, 2020). It has been demonstrated by similar thermo-mechanical models that realistic upper plate topography can be only achieved when a low viscosity mantle wedge is implemented (Billen and Gurnis, 2001). In our models, dehydration of the down-going slab leads to the development of a weak and hydrated mantle wedge, furthermore, the subduction interface strength is also connected to the amounts of subducted weak sediments (Behr and Becker, 2018; Sobolev and Brown, 2019; Brizzi et al., 2020; Balázs et al., 2021a). Our models with different erosion and sedimentation rates (Figs. 8-9) show that the higher imposed sedimentation and thicker sediment accumulation in the subduction interface lead to lower interface strength, hydrating and weakening the overlying lithosphere and thus create less efficient stress transfer towards the upper plate. Sediments or crustal slivers are also accumulating beneath the forearc high contributing to its Myr-scale periodic vertical motions (Fig. 7; Menant et al., 2020).

Previous studies suggested that lubrication of the subduction interface by sediments leads to increased subduction velocities during free-fall subduction (Behr and Becker, 2018; Sobolev and Brown, 2019). Our 2D simulations show the opposite effect, in agreement with the recent 3D simulations by Munch (2020) and 2D studies by Brizzi et al. (2021). Higher erosion and sedimentation rates lead to erosional unloading of the forearc high and contributes to additional sedimentary loading of the trench and lower plate. This material re-distribution leads to the following effects: (1) increased sediment subduction decreases the averaged density of the downgoing plate and decreases the slab pull force (cf., Brizzi et al., 2021), (2) the larger accretionary wedge increases the friction between the lower and upper plate and this leads to mechanical locking of the interface (Munch 2020), (3) material re-distribution modifies the slab curvature radius (Fig. 8) and decreases the resistance of the slab against bending (cf., Buffett 2006). The first two effects favor a slower subduction, while the latter would cause subduction acceleration. Our models infer that the first two effects overcome the decreased slab bending resistance and therefore increased sedimentation leads to an overall lower subduction velocity compared with the models with lower sedimentation rate. This is important for the topographic response because the higher subduction velocity leads to higher negative dynamic topographic effect by ca. 2 km (Fig. 9). These preliminary results need to be justified by further 2D and 3D models incorporating elasto-visco-plastic rock rheologies and exploring wider range of rheological properties, sediment densities and other subducted rocks, which may alter the coupling and density structure of the forearc.

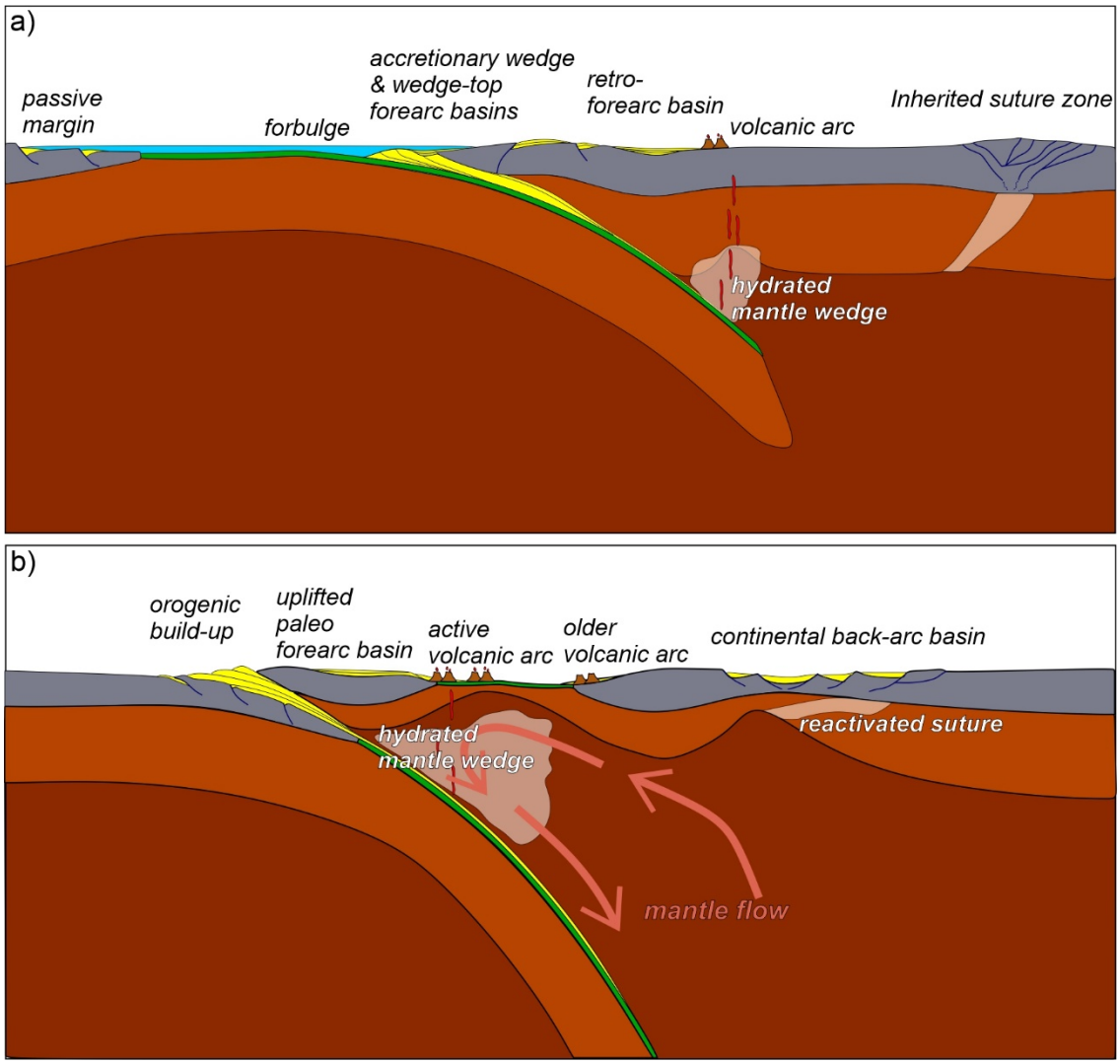

Figure 11. Simplified evolutionary model for the location of forearc and back-arc basins. a) Early stage of oceanic subduction is associated with the development of wedge-top forearc basins and negative residual topography in the retro-forearc basin, volcanism above the hydrated mantle wedge and incipient strain localization along inherited structures. b) During the mature stage of oceanic and early phase of continental subduction the forearc basins are uplifted and back-arc basins are formed by reactivation of the inherited weak structures or between the older volcanic and the new volcanic arc following arc rifting. c) Subsidence history of the back-arc basin. d) Subsidence history of the forearc basin. SCOL – soft collision, STZ – slab mantle zone interaction.

1. **Forearc and back-arc sedimentary basin classification and subsi-**

dence history

Our models propose two different viable scenarios for forearc and back-arc basin evolution. Depending on which rheological weakening mechanisms is more effective, back-arc basins either form following arc rifting and rapidly leading to oceanic spreading or includes a long-lasting continental stretching phase followed by oceanic break-up (Fig. 11). Basin formation starts similarly in every model, leading to the development of the accretionary wedge and related wedge-top deformation and wedge-top forearc basin subsidence under variable compression and extensional pulses within the forearc region (Fig. 3a-c). Furthermore, accommodation space is created in the syncline structure of the retro-forearc basin. This means that forced subduction initiation leads to an earlier stage of retro-forearc basin subsidence prior to back-arc basin formation and subsidence. Thereafter, the slab reaches a greater depth of ca. 400 km and slab-roll back and trench retreat results in extensional stress field in the upper plate. In the models where a volcanic arc formation is simulated trench retreat is first accommodated by distributed normal faulting but deformation rapidly shifts to and localizes in the volcanic arc region leading to arc-rifting (Fig. 7c). Subsequent rapid roll-back and trench retreat is accommodated by fast rifting and subsequent break-up. Lithospheric break-up occurs at ca. 130 km distance from the initial volcanic arc within the former forearc syncline (Fig. 7c). This break-up drifts the initial forearc basin into the two opposite passive margins of the newly formed back-arc ocean. Fast back-arc spreading continues until slab break-off (Figs. 7d, 10). This evolutionary model agrees with the classical models proposed for back-arc ocean development (cf., Karig 1971; Baitsch-Ghirardello et al., 2014; Billen, 2017).

In the models with inherited upper plate weak zones extensional stress is transferred towards to upper plate at larger distances and deformation localizes along the weak zone (Fig. 3). Wedge-top and retro-forearc basin subsidence is similar to the previous scenario (Figs. 3, 10), but a long-lasting back-arc rifting stage precedes back-arc oceanic spreading in case of a long oceanic subduction, while a shorter oceanic subduction stage only enables the development of an intra-continental extensional back-arc basin (cf., Figs., 3-4). Onset of forearc subsidence is also earlier in this scenario than the onset of extensional back-arc subsidence, however, back-arc extension and rifting last longer, also during the first million years of soft collision and continental subduction. While soft collision, i.e, arrival of the extended passive margin into the subduction zone leads to rapid uplift of the trench and forearc regions, this would correspond to the transition from deep marine *flysch* to continental *molasse* sedimentation (Figs. 3, 11). Furthermore, the forearc region undergoes trench-ward tilting during fast trench retreat and rapid uplift when the slab reaches the bottom of the upper mantle (Figs. 3-4). Finally, hard collision, i.e., arrival of the thick continental lower plate leads to the cessation of back-arc extension and marks the onset of thick-skinned orogenic build-up prior to slab break-off (Fig. 3f).

1. **Driving forces of forearc and back-arc basin subsidence and uplift**

The presented model series enable the discussion of the main driving forces controlling forearc and back-arc basin subsidence. Subsidence of the retro-forearc basin is not isostatically compensated, as its 2-4 km tectonic subsidence occurs in the absence of notable crustal thickness variations. Our models show that this region gradually subsides from the onset of forced subduction and the amount and rates of its subsidence is linked to many parameters including the strength of the subduction interface, elasticity of the upper plate, and the amount of subduction, slab dip angle and slab geometry in the mantle. It has been shown by previous similar studies that elasticity plays a major role in the distribution and magnitude of deviatoric stress and thus controls subduction dynamics and related topography (Zhong and Gurnis, 1994; Farrington et al., 2014; Fourel et al., 2014; Bessat et al., 2020). In our models, elasticity contributes to greater initial retro-forearc subsidence in the syncline structure of the upper crust during the early trench advance phase of incipient subduction (cf., Figs. 3a, 7a). Furthermore, elasticity also contributes to larger slab curvature radius modifying slab dip and dynamics and thus upper plate deformation (cf., Lallemand et al., 2005). Following this early stage of compression induced flexural subsidence, retro-forearc subsidence is driven by the downward pulling of the slab by trench suction force (Fig. 1), i.e., the gradually steepening slab drags down the overlying upper plate (Elsasser, 1971; Forsyth and Uyeda, 1975). The locus of the retro-forearc depocenter overlies the deepest contact point of the subduction interface (Fig. 3). This implies that subsidence is mainly driven by vertical stresses imposed at the base of the upper plate transmitted through the interface (e.g., Buiter et al., 2001; Billen and Gurnis, 2001; Chen et al., 2017). This agrees with our results of models with different amounts of subducted sediments, where a thicker sediment accumulation in the interface lowers its strength and leads to lower stress accumulation in the upper plate that is associated with lower forearc subsidence (Fig. 8-9). It has been also shown by previous models that this subsidence and the vertical stresses acting on the base of the upper plate are linked to the buoyancy of the slab (Crameri et al., 2017). Our models also show that gradual slab steepening contributes to forearc subsidence (cf., modhom in Fig. 6) due to the increasing buoyancy force of the deeper slab and increased stress transfer towards the upper plate over the interface. This means that the gradually steepening slab drags down the upper plate above the subduction interface. This explains why a steeper slab geometry results in larger forearc subsidence after the same amount of subduction (Fig. 5).

An important stage of forearc evolution shows the gradual trench-ward tilting of the upper plate during mature subduction (Fig. 3d) that is associated with the subsidence of the former forearc high and corresponds to the slow uplift of the retro-forearc depocenter. A similar tilting process is simulated by previous models during slab-transition-zone interaction, and it is proposed that upper plate tilting is caused by the larger-scale mantle flow pattern by excitation of the high-viscosity lower mantle (Crameri and Lithgow-Bertelloni, 2018). Analogue models simulating solely the upper mantle reported a similar tilting event that is linked to variations in the vertical component of the trench suction along

the interface during steady state slab roll-back (Chen et al., 2017). In our simulations upper plate trench-ward tilting commences prior the leading edge of the slab reaches the bottom of the model, during free-fall stage (Fig. 3d, Fig S2 in the supplementary material). This gradual tilting is observed from the onset of high-rate trench retreat and slab roll-back. During this phase the slab dip angle becomes lower, the S-point retreats and thus slab suction or drag will be more dominant in the shallower parts of the interface compared to the preceding slab steepening stage. In the model, where the upper plate is strong without any weak zones, the trench retreat and slab roll-back is suppressed compared with the reference model, and in this case the forearc region records continuous subsidence until the slab reaches the bottom of the model (Fig. 6 b,c). This implies that upper plate tilting is connected to the onset of the retreating trench and the termination of slab steepening. Tilting may also be partly related to some internal rigidity of the rapidly retreating forearc, which experiences counter-clockwise rigid-body rotation when its leading-edge rides over less steep regions of the subducting plate.

Our modelling results confirm that extensional back-arc basin subsidence is primarily controlled by crustal thinning driven by the retreating subduction trench relative to the upper plate (Figs. 1, 11). Slab roll-back, trench retreat and extensional back-arc basin formation are connected to mantle flow and the buoyancy of the slab (Conrad and Hager, 1999; Wallace et al., 2009; Magni et al., 2014; Faccenna et al., 2014). When the convergence velocity remains low, subduction is partitioned into slab roll-back (Fig. 10). Trench retreat and back-arc extension require a weak upper plate. Previous models either proposed high thermal gradients (Gogus, 2015; Wolf and Huismans, 2019; Erdos et al., 2021; Balázs et al., 2021a), assumed inherited crustal nappes or mantle weak suture zones (Menant et al., 2016; Balázs et al., 2021b; Yang et al., 2021) or rheological weakness created by the evolving hydrated mantle wedge and volcanic arc (Baitsch-Ghirardello et al., 2014; Magni, 2019). During gradual roll-back and back-arc extension, the lithosphere of the upper plate gradually thins and thus its strength decreases contributing to speed up the back-arc extension (Fig. 10). Finally, long wavelength dynamic topography is superimposed on the previous, shorter wavelength processes driven by vertical stresses imposed at the base of the upper plate driven by the underlying mantle flow (e.g., Husson, 2006; Faccenna and Becker, 2020). This effect is best illustrated in our free-fall subduction model (Fig. 9). The regularly increasing mantle flow velocities from 1.5 to 7.1 cm/yr gradually deflects the topography in the vicinity of the trench for both the lower and upper plates leading to an additional subsidence of ca. 1.7 km over a wavelength of 750 km. This corresponds to deepening of the trench and trench-ward tilting of the upper plate (Fig. 9). Therefore, our models simulate a shorter wavelength flexural and trench suction related forearc subsidence and a mantle flow driven larger wavelength dynamic topographic signal.

1. **Model limitations and outlook**

Our high-resolution models only simulate the upper mantle until 660 km (excluding sticky air) with a free-slip lower boundary. Complex slab – transition zone and lower mantle effects are not considered. Such an assumption is often used because of the significant viscosity increase in the lower mantle (e.g., Conrad and Hager, 1999) and the limited timescale of the modelled subduction history (Davies 1995; Funiciello et al., 2003). In our 2D setup 3D mantle flow effects cannot be simulated, although it has been shown that toroidal mantle flow plays a major role in back-arc extension, while our models overestimate the poloidal mantle flow component. Our regional-scale model domain only allowed the simulation of one slab, while global 3D subduction models (e.g., Tackley, 2000; Coltice et al., 2019) also address more complex slab and mantle flow interactions. The simulations including melt extraction only handled visco-plastic rheologies.

4.5 Comparison with Mediterranean subduction zones

We compare our model results with the evolution of forearc and back-arc basins formed on the overriding plates of Mediterranean subduction zones. The Pannonian-Transylvanian, Tyrhenian-Paola, Western and Eastern Alboran, North and South Aegean basins formed in response to the retreat of the Carpathian, Ionian, Gibraltar and Hellenic slabs during the formation of the Carpathians, Apennines, Betics-Rif and Hellenides orogens, respectively (e.g., Faccenna et al., 2014). Despite the similarities of these subduction zones (Fig. 12) they show different amounts and rates of upper and lower plate velocities and convergent rates that resulted in different amounts of upper plate extension values.

4.5.1 Evolution of the Pannonian-Transylvanian-Carpathians system

The Pannonian-Transylvanian Basin is surrounded by the Alpine-Carpathians-Dinarides orogens in Central Europe (Fig. 12). The Pannonian Basin is floored by 22-25 km thinned continental crust including in average 2-4 km thick Miocene to Recent sediments (Kalmár et al. 2021). The basin overlies an attenuated lithosphere of ca. 50-60 km resulting 100-120 mW/m^2 high surface heat flow (Tari et al., 1999; Lenkey et al., 2002; Horváth et al. 2015). In contrast, the Transylvanian Basin has ca. 35 km thick crust, and a lower surface heat flow of 45 mW/m^2, only the closest vicinity of volcanic edifices shows high 110 mW/m^2 values (Tilita et al. 2013).

The formation of the Pannonian and Transylvanian Basins followed the Mesozoic opening and subsequent closure of two oceanic realms connected to the evolution of the larger Neotethys and the Alpine Tethys oceans. The Neotethyan branch opened during the Middle Triassic and was closed by late Jurassic-Cretaceous subduction and collision resulting in a suture in the transition between the present-day Pannonian Basin and Dinarides, creating the Sava suture zone. The area presently enclosed by the Carpathians was occupied by the land-locked partly oceanic and partly continental hyperextended basin, that formed during the Jurassic related to the Alpine Tethys spreading and its subduction was ini-

tiated in the Late Cretaceous. The upper plate of the Carpathian embayment subduction was composed of two megaunits with different paleogeographic origin. The AlCaPa megaunit in the north derived from the Alpine orogenic wedge, while Tisza-Dacia in the South detached from the Dinaridic margin (Fig. 12b; Csontos and Vörös, 2004; Schmid et al., 2008; Matenco and Radivojevic, 2012; Horváth et al., 2015). This pre-rift orogenic evolution resulted in similar crustal or mantle inherited weak zones as the implemented ones in our and similar numerical models (Fodor et al., 2021).

Recent, narrow remnant of the slab connected to the formation and evolution of the Pannonian-Transylvanian basins is presently imaged beneath the SE Carpathians (Wortel and Spakman, 2000) and it is in the process of break-off (Ismail-Zadeh et al., 2012). Eastward, ca. 200-300 km slab rollback accommodated the extension of the Pannonian back-arc basin. Age of the oldest syn-rift sediments, exhumation ages of metamorphic cores and ages of calc-alkaline volcanism infers a ca. 20-22 Myr onset of extension that was first localized along the inherited Sava suture zone along the Dinaridic margin and deformation gradually migrated towards the center of the basin until ca. 9 Ma (Ustaszewski et al., 2008; Matenco and Radivojevic, 2012; Horváth et al., 2015; Lukács et al., 2018; Balázs et al., 2021b).

Different evolutionary models have been proposed for the subsidence of the Transylvanian Basin. Crustal down-warping due to the pull of the retreating slab was proposed by Royden et al. (1982) to explain the Miocene non-extensional subsidence of the basin. Krezsek and Bally (2006) proposed a multi-stage evolution, including Upper Cretaceous rifting and subsequent inversion and Paleogene sagging, followed by Lower Miocene flexural basin development and gravitational spreading. Later studies (Matenco and Radivojevic, 2012, Tilita et al. 2015) emphasized the connection between the evolution of the Pannonian and Transylvanian Basins by lithospheric-scale simple shear mechanism and lower crustal flow effects. The late Miocene to Recent uplift of the Transylvanian Basin is interpreted to be the effect of the ongoing slab detachment beneath the SE Carpathians (Wortel and Spakman, 2000) coupled with mantle delamination (Gogus and Ueda, 2018) and further mantle flow effects (Sengul-Uluocak et al., 2019) and related volcanism (Gartner et al., 2020).

Our model results with a smaller oceanic basin are in agreement with the crustal and lithospheric thinning and extensional back-arc subsidence of the Pannonian Basin and the notable non-extensional subsidence and late-stage uplift of the Transylvanian Basin. Onset of compression induced subsidence in the forearc is coeval with back-arc contraction and uplift caused by forced subduction initiation (Fig. 3). During mature subduction, the inherited weak zone localized extensional deformation resulting in crustal and mantle thinning and back-arc basin subsidence, while continuous sag subsidence took place in the forearc basin driven by slab steepening and downward suction. Continental subduction marked the uplift of the forearc basin, while back-arc extension continued until hard collision. The model with the converging upper plate (Modtwfr; Fig. 5)

enables the most suitable comparison with the kinematics of the Carpathian subduction zone. After the convergence velocity is 0 cm/yr, slab roll-back is purely accommodated by upper plate extension creating a continental extensional basin, the forearc is subsiding driven by the suction of the retreating slab. Finally, when the slab roll-back velocity ceases, the back-arc basin still subsides driven by thermal cooling, while the forearc basin records uplift due to the ongoing mantle convection and by the onset of slab necking prior to break-off.

4.5.2 Evolution of the Calabrian-Tyrrhenian system

The Tyrrhenian back-arc, Paola forearc basins and the Calabrian accretionary wedge in the central Mediterranean formed during the Neogene subduction and trench roll-back of the Ionian oceanic slab (Fig. 12c). Seismic tomography and previous reconstruction infer ca. 1000 km subduction and 800 km trench retreat besides the additional 200 km plate convergence in the case of the southern Tyrrhenian since 30 Ma (e.g., Faccenna et al., 2014). The relict of the originally larger subduction zone is imaged today as a narrow, deep and steep NW dipping slab (Faccenna et al. 2014 and references therein). Trench retreat was accommodated by upper plate extension and crustal thinning of the Tyrrhenian Basin leading to the overall eastward migration of deformation (e.g., Rosenbaum and Lister, 2004; Minelli and Faccenna, 2010; Loreto et al., 2021).

Crustal thickness in the region gradually thins from 40 km in Calabria to 30 km below the Paola Basin, the latter hosts ca. 4.5 km thick Plio-Quaternary sediments in an overall syncline geometry (Corradino et al., 2020). Further west towards the Tyrrehnian Sea crustal thickness gradually decreases and is entirely attenuated in the Vavilov and Marsili Basins leading to mantle exhumation and localized spreading (Fig. 12c; Nicolosi et al., 2006). Surface heat flow is ca. 50-80 mW/m^2 in the Paola Basin, while in the Thyrrenian Basin this value reaches 150-250 mW/m^2 due to the attenuated lithosphere (Zito et al., 2003).

Similar to our model results trench retreat shows an initial slow velocity for the first 10 Myr of subduction from 15 Ma, slab roll-back and trench retreat fastens between 6-3 Ma and slow down again from 3 Ma to present (Minelli and Faccenna, 2010). Highest trench retreat velocity is inferred during the opening of the Vavilov and Marsili Basins, reaching higher values between 2.1-1.6 Myr (Nicolosi et al., 2006). Similar dynamics is observed in our models, where the initial gradual increase of slab roll-back velocity is controlled by the gradually increasing slab-pull force and mantle return flow, while the subsequent velocity decrease is simulated after the slab reaches the bottom of the upper mantle and during the following continental subduction (Fig. 10). Furthermore, highest roll-back velocities are observed during the last stages of back-arc rifting and during back-arc spreading when the upper plate strength and related resistance becomes suppressed (Figs 5c, 10). In agreement with our models (Figs. 4-5) extensional deformation was initially distributed over a larger area, initially located at a larger distance from the subduction zone and subsequently migrated towards the volcanic arc (e.g., Rosenbaum and Lister, 2004; Loreto et al., 2021). While subsidence of the Tyrrhenian Basin was controlled by exten-

sion and crustal thinning, subsidence of the Paola Basin is not accommodated by major normal faults (Pepe et al., 2010). Its syncline geometry and its position between the Aeolian Volcanic arc and the accretionary wedge infers its tectonic origin as a similar retro-forearc basin as in our models (Fig. 9; Corradino et al., 2020) controlled by moderate contraction and slab suction being coeval with the extension of the Tyrrhenian back-arc basin.

4.5.3 Evolution of the Alboran system

Evolution of the western Mediterranean region is confined by the interaction between the larger African and Eurasian plates and the Iberian plate, the latter moved independently between the Early Jurassic and Oligocene (Jimenez-Munt et al. 2019). Surrounded by these plates, subduction of an oceanic segment of the Alpine Tethys slab resulted in the formation of the west Alboran forearc basin and the east Alboran and Algerian extensional back-arc basins (Do Couto et al. 2016). The remnant of this slab is imaged today beneath the western Alboran Sea and southern Spain (Fig. 12). The 3D complexity of this region led to still debated tectonic reconstructions (e.g., Faccenna et al., 2014; Spakman and Wortel, 2004; Verges and Fernandez, 2012). Our simplified 2D models do not aim to decipher the complex 3D paleogeographic history of the Alboran domain but contributes to understand the subsidence and uplift patterns of the forearc and back-arc basins of this subduction zone.

Highest crustal thickness in the region is measured beneath the Gibraltar arc reaching ca. 45 km. An imbricated sedimentary wedge is formed in the Gulf of Cadiz overlying the Atlantic oceanic domain. The crustal thickness gradually decreases eastwards having 30-40 km beneath the Eastern Alboran Basin and evolves into a thinned continental and oceanic crust towards the Western Alboran and Algerian Basin, respectively (Fig. 12c; Comas et al., 1999; Villasenor et al., 2015). The East Alboran Basin has a lower thermal gradient and a lower surface heat flow of ca. 40-80 mW/m^2, while this is up to 130 mW/m^2 in the western Alboran Basin reflecting the gradual lithospheric thinning towards the most extended back-arc domain (Torne et al., 2000).

Similar to the above mentioned Transylvanian and Paola basins, the evolution of the Western Alboran Basin has been debated and has been considered either as a back-arc basin or forearc basin (Do Couto et al., 2016; d'Acremont et al., 2020). Our model results are in agreement with high resolution seismic interpretation (Fig. 12d) inferring the forearc nature of the Western Alboran Basin implying slab suction and compression as the main basin forming mechanisms, while back-arc extensional deformation was localized at larger distances within the Eastern Alboran and Algerian basins.

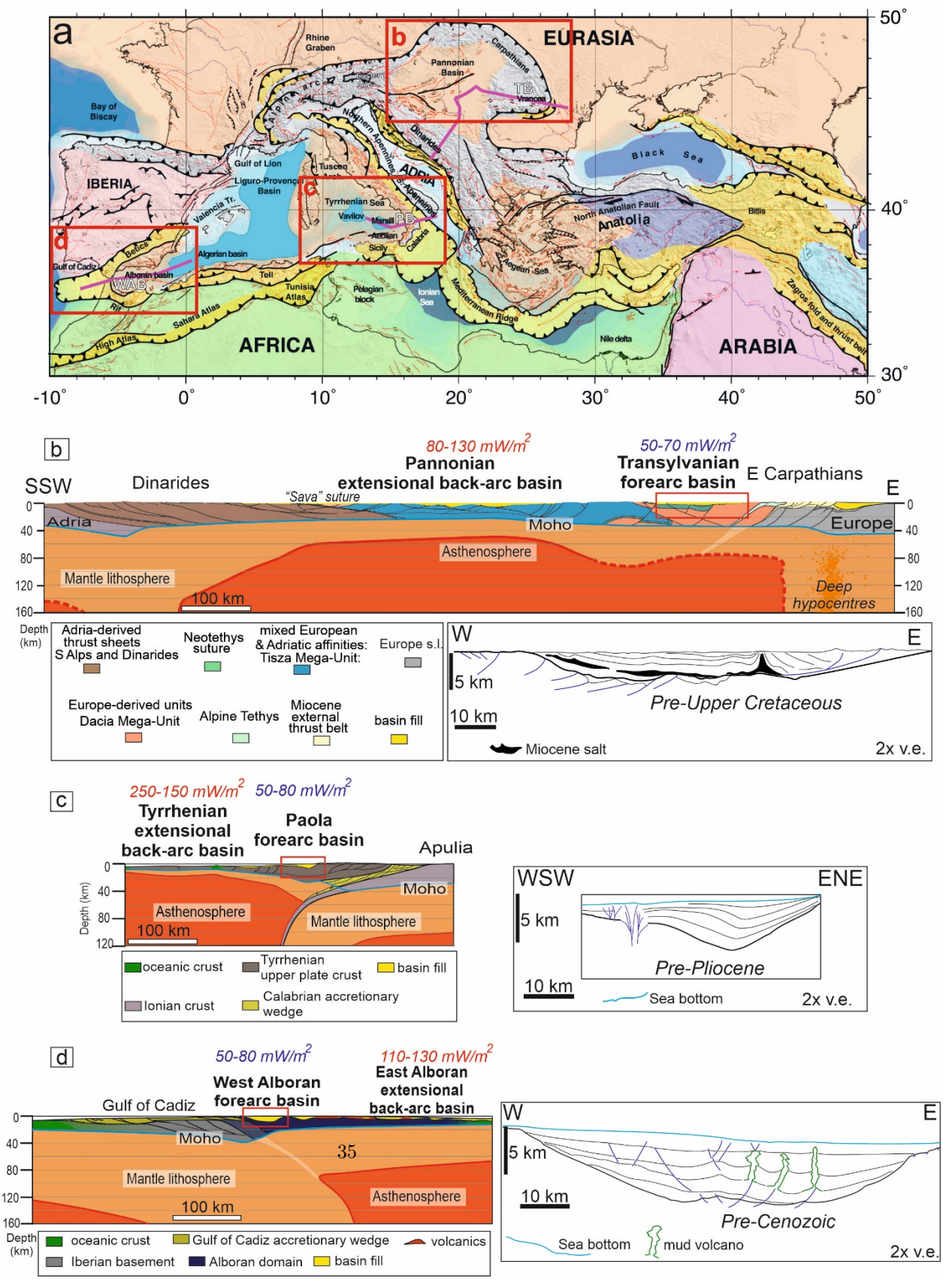
a
b
c
d
EURASIA
AFRICA
ARABIA
IBERIA
ADRIA
Rhine Graben
Pannonian Basin
Carpathians
TB
Vrancea
Bay of Biscay
Alpine arc
Northern Apennines
Dinarides
Black Sea
Gulf of Lion
Tuscan Arch
Liguro-Provençal Basin
Tyrrhenian Sea
Vavilov
Marsili
PB
Aeolian
Sicily
Calabria
Apennines
Valencia Tr.
Betics
Algerian basin
Gulf of Cadiz
Alboran basin
WAB
Rif
Tell
Tunisia Atlas
Sahara Atlas
High Atlas
Pelagian block
Ionian Sea
Mediterranean Ridge
Aegean Sea
North Anatolian Fault
Anatolia
Bitlis
Zagros fold and thrust belt
Nile delta
50°
40°
30°
-10°
0°
10°
20°
30°
40°
50°
b
SSW
Dinarides
"Sava" suture
80-130 mW/m2
Pannonian
extensional back-arc basin
50-70 mW/m2
Transylvanian
forearc basin
E Carpathians
E
Adria
Moho
Europe
Asthenosphere
Mantle lithosphere
100 km
Deep
hypocentres
Depth
(km)
0
40
80
120
160
Adria-derived
thrust sheets
S Alps and Dinarides
Neotethys
suture
mixed European
& Adriatic affinities:
Tisza Mega-Unit:
Europe s.l.
Europe-derived units
Dacia Mega-Unit
Alpine Tethys
Miocene
external
thrust belt
basin fill
W
E
5 km
10 km
Pre-Upper Cretaceous
Miocene salt
2x v.e.
c
250-150 mW/m2
50-80 mW/m2
Tyrrhenian
extensional
back-arc basin
Paola
forearc basin
Apulia
Moho
Asthenosphere
Mantle lithosphere
100 km
Depth (km)
0
40
80
120
oceanic crust
Tyrrhenian
upper plate crust
basin fill
Ionian crust
Calabrian accretionary
wedge
WSW
ENE
5 km
10 km
Pre-Pliocene
Sea bottom
2x v.e.
d
50-80 mW/m2
West Alboran
forearc basin
110-130 mW/m2
East Alboran
extensional
back-arc basin
Gulf of Cadiz
Moho
35
Mantle lithosphere
100 km
Asthenosphere
Depth
(km)
0
40
80
120
160
oceanic crust
Gulf of Cadiz accretionary wedge
volcanics
Iberian basement
Alboran domain
basin fill
W
E
5 km
10 km
Pre-Cenozoic
Sea bottom
mud volcano
2x v.e.

Figure 12. (a) Tectonic map of the Mediterranen (after Faccenna et al., 2014). Lithospheric-scale cross-sections and line drawing interpretation of seismic sections from the Transylvanian-Pannonian Basins (compiled after Tari et al., 1999; Krezsek et al., 2006; Matenco and Radivojevic, 2012; Tilita et al., 2013; Schmid et al., 2008; Horváth et al., 2015; Balázs et al., 2018), Paola-Tyrrhenian Basins (compiled after Zito et al., 2003; Minelli and Faccenna, 2010; Pepe et al., 2010; Corradino et al., 2020) and Western and Eastern Alboran Basins (compiled after Comas et al., 1999; Medialdea et al., 2004; Do Cuoto et al., 2016; Jimenez-Munt et al. 2019, d'Acremont et al., 2020). Note the wide syncline structure of the similar retro-forearc basins having 50-80 mW/m^2 surface heat flow and the extended back-arc basins having thinned crust and high heat flow.

5. Conclusions

The dynamics of oceanic and continental subduction zones influences the rise and demise of forearc and back-arc sedimentary basins of the overriding plate. Subsidence and uplift rates of these distinct basins are controlled by variations in plate convergence and subduction velocities and determined by the rheological and thermal structure of the lithosphere. In this study we conducted a series of high-resolution 2D numerical models of oceanic subduction and subsequent continental collision. Our model results led to the following main conclusions.

Both the onset and cessation of subsidence in the forearc and backarc basins are diachronous. Horizontally forced subduction initiation leads to earlier forearc subsidence. Soft collision leads to forearc uplift, while back-arc subsidence continues until hard collision. The forearc region of oceanic subduction zones is characterized by repeated contraction and extension phases. Accommodation space and sedimentary basins are formed on top of the accretionary wedge creating piggy-back or wedge-top forearc basins, while retro-forearc basins are formed on the overriding continental plate in a wide syncline structure overlying the subduction interface at ca. 200 km distance from the accretionary wedge between a forearc high and the volcanic arc. The volcanic arc in our models initially form at ca. 250 km from the accretionary wedge. Forced subduction initiation and initial overriding plate compression results in a flexural proto-forearc basin its syn-kinematic sedimentary age can constrain the age of subduction initiation.

The retro-forearc subsidence is amplified by gradually increasing slab-pull force acting on the slab and trench suction of the overriding plate. A weaker subduction interface, e.g., by enhanced sediment subduction enables less efficient stress transfer and leads to lower forearc subsidence. During mature free-fall subduction and the climax of slab roll-back the forearc high subsides beneath sea-level and the locus of the forearc depocenter migrates trench-ward reflected by upper plate tilting. Models simulating free-fall subduction of a mobile lower plate led to high subduction and mantle flow velocities up to 7 cm/yr and results in the highest negative dynamic topographic signal within the trench and in the upper plate. Ultimately, continental subduction or after the slab reaches the bottom of the upper mantle, the forearc basin records rapid uplift.

The back-arc region of the upper plate records compression or extension based on the dynamics of subduction and convergence velocities. Back-arc subsidence is mainly controlled by crustal thinning governed by slab roll-back. Back-arc deformation localizes in the upper plate along inherited crustal or mantle weak zones often 100s of kilometers from the trench. Gradual hydration of the mantle wedge and the evolution of a volcanic arc and related melt-induced weakening also favors strain localization and intra-arc deformation followed by the trenchward migration of deformation and volcanism following slab roll-back. Back-arc extension velocity gradually increases by the increasing slab pull and increasing mantle return flow effect, further facilitated by the gradually decreasing strength of the progressively thinned overriding plate. Back-arc spreading marks a sudden acceleration of back-arc extension. Soft collision and early stages of continental subduction led to the abrupt uplift of the forearc basin, while trench retreat and back-arc extension continuous until hard collision when slab-pull and mantle flow controls are overtaken by the buoyancy force of the subducted continental crust.

Our modelling results provide insights into the evolution of Mediterranean subduction zones and propose that the Western-Eastern Alboran, Paola-Tyrrhenian, Transylvanian-Pannonian Basins should be considered as genetically connected forearc –back-arc basins, respectively.

Acknowledgements

All numerical models were run on the Euler and Leonhard clusters at ETH Zurich. AB acknowledges financial support from the ETH Zurich Postdoctoral Fellowship program. The Grant to Department of Science, Roma Tre University (Miur-Italy Dipartimenti di Eccellenza, Commi 314–337 Legge 232/2016) is acknowledged. We note that there are no data sharing issues since all the numerical information is provided in the figures created by solving the equations presented in the supplementary material.

References

Andrić, N., Vogt, K., Matenco, L., Cvetković, V., Cloetingh, S., & Gerya, T. (2018). Variability of orogenic magmatism during Mediterranean-style continental collisions: a numerical modelling approach. *Gondwana Res.*, 56, 119–134.

Balázs, A., Faccenna, C., Ueda, K., Funiciello, F., Boutoux, A., Blanc, E. J-P., & Gerya, T. (2021a). Oblique subduction and mantle flow control on upper plate deformation: 3D geodynamic modeling. *Earth and Planetary Science Letters,* 569, https://doi.org/10.1016/j.epsl.2021.117056

Balázs, A., Ma enco, L., Granjeon, D., Vogt, K., Francois, T., & Sztanó, O. (2021b). Towards stratigraphic thermo-mechanical numerical modelling: integrated analysis of asymmetric extensional basins. *Glob. Planet. Chang.*, 196, https://doi.org/10.1016/j.gloplacha.2020.103386.

Baitsch-Ghirardello, B., Gerya, T.V., & Burg, J-P., (2014). Geodynamic regimes of intra-oceanic subduction: Implications for arc extension vs.

shortening processes. *Gondwana Res.* 25, 546-560.

Behr, W.M., & Becker, T.W. (2018). Sediment control on subduction plate speeds. *Earth and Planetary Science Letters*, 502, 166–173. https://doi.org/10.1016/j.epsl.2018.08.057

Bessat, A., Duretz, T., Hetenyi, G., Pilet, S., & Schmalholz, S. M. (2020). Stress and deformation mechanisms at a subduction zone: Insights from 2-D thermomechanical numerical modelling. *Geophysical Journal International*, 221, 1605–1625. https://doi.org/10.1093/gji/ ggaa092

Billen, M.I., & Gurnis, M. (2001). A low viscosity wedge in subduction zones. *Earth and Planetary Science Letters,* 193, 227-236.

Billen, M. I. (2017). Insights Into the Causes of Arc Rifting From 2-D Dynamic Models of Subduction. *Geophysical Res. Let.,* 44, 10948-10957.

Braun, J. (2010). The many surface expressions of mantle dynamics. *Nature Geoscience*, 3, 825-833.

Brizzi, S., van Zelst, I., Funiciello, F., Corbi, F., & van Dinther, Y. (2020). How sediment thickness influences subduction dynamics and seismicity. *Journal of Geophysical Research: Solid Earth*, 125, e2019JB018964. https://doi.org/10.1029/2019JB018964

Brizzi, S., Becker, T.W., Faccenna, C., van Zelst, I., & van Dinther, Y. (2021). Control of sediments on subduction dynamics and geometry. *Manuscript submitted to Geophysical Research Letters.*

Brune, S., Williams, S. E., Butterworth, N. P., & Müller, R. D. (2016). Abrupt plate accelerations shape rifted continental margins. *Nature*, **536**, 201– 204.

Buffett, B. A. (2006). Plate force due to bending at subduction zones. *Journal of Geophysical Research: Solid Earth*, 111, B09405, doi:10.1029/2006JB004295

Buiter, S. J. H., Govers, R., & Wortel, M. J. R. (2001). A modeling study of vertical surface displacements at convergent plate margins. *Geophysical Journal International*, 147, 415–427. https://doi.org/10.1046/j.1365-246X.2001.00545.x

Burov, E. (2011). Rheology and strength of the lithosphere. *Marine and Petroleum Geology* 28, 1402-1443.

Capitanio, F.A., Stegman, D.R., Moresi, L.N., & Sharples, W. (2010). Upper plate controls on deep subduction, trench migrations and deformations at convergent margins. *Tectonophysics*, 483, 80–92.

Cerpa, N.G. & Arcay, D. (2020). Overriding Plate Velocity Control on Surface Topography in 2-D Models of Subduction Zones. *Geochemistry, Geophysics, Geosystems*, 21, e2019GC008900

Chen, Z., Schellart, W., Duarte, J. & Strak, V. (2017). Topography of the overriding plate during progressive subduction: a dynamic model to explain forearc subsidence. *Geophys. Res. Lett.*, 44, 9632-9643.

Cizkova, H. & Bina, C.R. (2013). Effects of mantle and subduction-interface rheologies on slab stagnation and trench rollback. *Earth and Planetary Science Letters*, 379, 95-103.

Coltice, N., Laurent, H., Faccenna, C. & Maëlis, A. (2019). What drives tectonic plates? *Sci. Adv.* 5, 4295. https://doi .org /10 .1126 /sciadv.aax4295.

Comas, M.C., Platt, J.I., Soto, J.J. & Watts, A.B. (1999). The origin and tectonic history of the Alboran Basin: Insights from Leg 161 results, in *Proc. Ocean Drill. Program*, 161, 555-579.

Conrad, C. P., & Hager, B. H. (1999). Effects of plate bending and fault strength at subduction zones on plate dynamics. *Journal of Geophysical Research: Solid Earth*, 104, 607 17551-17571.

Corradino, M., Pepe, F., Bertotti, G., Picotti, V., Monaco, C. & Nicolich, R. (2020). 3-D architecture and Plio-Quaternary evolution of the Paola Basin: Insights into the forearc of the Tyrrhenian-Ionian subduction system. *Tectonics*, 39, e2019TC005898. https://doi.org/10.1029/2019TC005898

Crameri, F., Schmeling, H., Golabek, G. J., Duretz, T., Orendt, R., Buiter, S. J. H., et al. (2012). A comparison of numerical surface topography calculations in geodynamic modelling: An evaluation of the 'sticky air' method. *Geophysical Journal International*, 189(1), 38–54. https://doi.org/10.1111/j.1365-246X.2012.05388.x.

Crameri, F., Lithgow-Bertelloni, C.R. & Tackley, P.J. (2017). The dynamical control of subduction parameters on surface topography. *Geochemistry, Geophysics, Geosystems, 18*, 1661-1687.

Crameri, F. & Lithgow-Bertelloni, C. (2018). Abrupt upper-plate tilting during slab-transition-zone collision. *Tectonophysics*, 746, 199-211.

Csontos, L. & Vörös, A. (2004). Mesozoic plate tectonic reconstruction of the Carpathian region. *Palaeogeography, Palaeoclimatology, Palaeoecology*, 210(1), 1–56. https://doi.org/10.1016/j.palaeo.2004.02.033

d'Acremont, E., Lafosse, M., Rabaute, A., Teurquety, G., Do Couto, D., Ercilla, G., et al. (2020). Polyphase tectonic evolution of fore-arc basin related to STEP fault as revealed by seismic reflection data from the Alboran Sea (W-Mediterranean). *Tectonics, 39*, e2019TC005885. https://doi.org/10.1029/2019TC005885

Dal Zilio, L., Faccenda, M., & Capitanio, F. (2018). The role of deep subduction in supercontinent breakup. *Tectonophysics*, 746, 312-324

Davies, G.F. (1981). Regional compensation of subducted lithosphere: Effects on geoid, gravity and topography from a preliminary model. *Earth Planet. Sci. Lett.*, 54, 431-441

Davies, G. F. (1995). Penetration of plates and plumes through the mantle transition zone, *Earth Planetary Sci. Lett.*, 133, 507–516.

Dickinson, W. R., & Seely, D. R. (1979). Structure and stratigraphy of forearc regions. *AAPG Bulletin*, 63(1), 2–31.

Dymkova, D., Gerya, T. & Burg, J-P. (2016). 2D thermomechanical modelling of continent–arc–continent collision. *Gondwana Res.* 32, 138-150.

Do Couto, D., Gorini, C., Jolivet, L., Lebret, N., Augier, R., Gumiaux, C., et al. (2016). Tectonic and stratigraphic evolution of the Western Alboran Sea basin in the last 25 Myrs. *Tectonophysics*, 677-678, 280–311. https://doi.org/10.1016/j.tecto.2016.03.020

Elsasser, W.M. (1971). Seafloor spreading as thermal convection. *J. Geophys. Res.*, 76, 1101-1112,

Erdos, Z., Huismans, R., Faccenna, C. & Wolf, S.G. (2021). The role of subduction interface and upper plate strength on back-arc extension: application to Mediterranean back-arc basins. *Tectonics*, https://doi.org/10.1029/2021TC006795

Espurt,N., Funiciello, F.,Martinod, J.,Guillaume, B., Regard, V., Faccenna, C., & Brusset, S. (2008). Flat subduction dynamics and deformation of the South American plate: insights from analog modeling. *Tectonics* 27, TC3011. doi:10.1029/2007TC002175.

Faccenna, C., Giardini, D., Davy, P., & Argentieri, A. (1999). Initiation of subduction at Atlantic-type margins: Insights from laboratory experiments. *Journal of Geophysical Research: Solid Earth*, 104(B2), 2749-2766.

Faccenna, C., P. Molin, B. Orecchio, V. Olivetti, O. Bellier, F. Funiciello, L. Minelli, C. Piromallo & A. Billi (2011). Topography of the Calabria subduction zone (southern Italy): Clues for the origin of Mt. Etna, *Tectonics*, 30, TC1003, doi:10.1029/2010TC002694.

Faccenna, C., Becker, T. W., Auer, L. Billi, A., Boschi, L., Brun, J. P., Capitanio, F. A., Funiciello, F., Horvàth, F., Jolivet, L. Et al. (2014). Mantle dynamics in the Mediterranean, *Rev. Geophys.*, 52, 283–332, doi:10.1002/2013RG000444.

Faccenna, C. & Becker, T. (2020). Topographic expressions of mantle dynamics in the Mediterranean. *Earth Science Reviews*, 209, 103327

Farrington, R.J., Moresi, L.-N. & Capitanio, F.A. (2014). The role of viscoelasticity in subducting plates, *Geochem. Geophys. Geosyst.*, 15, 4291-4304. doi.org/10.1002/2014GC005507

Flament, N., Gurnis, M. & Muller, R. D. (2013). A review of observations and models of dynamic topography, *Lithosphere*, 5(2), 189–210.

Fodor, L., Balázs, A., Csillag, G., Dunkl, I., Heja, G., Jelen, B., Kelemen, P., Sz, Kover, Nemeth, A., Nyíri, D., Selmeczi, I., Trajanova, M., & Vrabec, M. (2021). Crustal exhumation and depocenter migration from the Alpine orogenic margin towards the Pannonian extensional back-arc

basin controlled by inheritance. *Glob. Planet. Chang.* 201, 103475. https://doi.org/10.1016/j.gloplacha.2021.103475

Forsyth, D.W. & Uyeda, S. (1975). On the relative importance of the driving forces of plate motion, *Geophys. J. Int., 43*, 163–200.

Fourel, L., Goes, S. & Morra, G. (2014). The role of elasticity in slab bending. *Geochem. Geophys. Geosys.* 15, 4507-4525.

Fuller, C.W., Willett, S.D., & Brandon, M.T. (2006). Formation of forearc basins and their influence on subduction zone earthquakes. *Geology, 34*, 65-68.

Funiciello, F., Faccenna, C., Giardini, D. & Regenauer-Lieb, K. (2003). Dynamics of re-treating slabs: 2. Insights from three-dimensional laboratory experiments. *J. Geophys. Res.*108 (B4), 2207. https://doi .org /10 .1029 /2001JB000896.

Gartner, B.A.J.J., Seghedi, I., Nikogosian, I.K. & Mason, P.R.D. (2020). Asthenosphere-induced melting of diverse source regions for East Carpathian post-collisional volcanism, *Contrib. Mineral. Petrol.*, 175, 54. 10.1007/s00410-020-01690-4

Gerya, T. V., & Yuen, D. A. (2007). Robust characteristics method for modelling multiphase visco-elasto-plastic thermo-mechanical problems. *Phys. Earth Planet. Inter.* 163, 83–105.

Gerya, T. V. (2010). Introduction to numerical geodynamic modelling (p. 345). Cambridge, UK: Cambridge University Press.

Gerya, T. V. & Meilick, F. I. (2011). Geodynamic regimes of subduction under an active margin: effects of rheological weakening by fluids and melts. *J Metamorph Geol, 29*, 7–31.

Göğüş, O. H. (2015). Rifting and Subsidence following lithospheric removal in continental back-arcs. *Geology, 43*, 3–6, doi:10.1130/G36305.1.

Gogus, O. H. & Ueda, K. (2018). Peeling back the lithosphere: Controlling parameters, surface expressions and the future directions in delamination modeling, *J. of Geodynamics*, 117, 21-40.

Gorczyk, W., Willner, A. P., Gerya, T. V., Connolly, J. A. D. & Burg, J.-P. (2007). Physical controls of magmatic productivity at Pacific-type convergent margins: Numerical modelling. *Phys. Earth Planet. Inter.* 163, 209–232

Holmes, A. (1944). Principles of Physical Geology. 189–190. Thomas Nelson and Sons.

Horváth, F., Musitz, B., Balázs, A. Végh, A. Uhrin, A. Nádor, A., Koroknai, B., Pap, N., Tóth, T. & Wórum, G. (2015). Evolution of the Pannonian basin and its geothermal resources. *Geothermics, 53*, 328–352.

Husson, L. (2006). Dynamic topography above retreating subduction zones. *Geology*, 34, 741-744.

Husson, L., Guillaume, B., Funiciello, F., Faccenna, C., & Royden, L.H. (2012). Unraveling topography around subduction zones from laboratory models. *Tectonophysics*, v. 526–529, p. 5–15, doi:10.1016/j.tecto.2011.09.001.

Ismail-Zadeh, A., Matenco, L., Radulian, M., Cloetingh, S. & Panza, G. (2012). Geodynamics and intermediate-depth seismicity in Vrancea (the south-eastern Carpathians): Current state-of-the art, *Tectonophysics*, 530, 50–79.

Jiménez-Munt, I., Torne, M., Fernàndez, M., Vergés, J., Kumar, A., Carballo, A., & García-Castellanos, D. (2019). Deep seated density anomalies across the Iberia-Africa plate boundary and its topographic response. *Journal of Geophysical Research: Solid Earth*, 124, https://doi.org/10.1029/

Kalmár, D. Hetényi, Gy., Balázs, A., & Bondár, I. (2021). Crustal thinning from orogen to back-arc basin: the structure of the Pannonian Basin region revealed by P-to-S converted seismic waves. *JGR-Solid Earth*, https://doi.org/10.1029/2020JB021309

Karig, D. E. (1971). Origin and development of marginal basins in the western Pacific, *J. Geophys. Res.*, 76(11), 2542–2561.

Krézsek, C., & Bally, A.W. (2006). The Transylvanian Basin (Romania) and its relation to the Carpathian fold and thrust belt: Insights in gravitational salt tectonics. *Mar. Petrol. Geol.* 23, 405—442.

Lallemand, S., A. Heuret & D. Boutelier (2005). On the relationships between slab dip, back-arc stress, upper plate absolutemotion, and crustal nature in subduction zones, *Geochem. Geophys. Geosyst.*, 6, Q09006, doi:10.1029/2005GC000917

Lenkey, L., Dovenyi, P., Horvath, F. & Cloetingh, S.A.P.L. (2002). Geothermics of the Pannonian Basin and its bearing on neotectonic. In: Cloetingh, S., Horvath, F., Bada, G., Lankreijer, A. (Eds.), Neotectonics and Surface Processes: the Pannonian Basin and Alpine/Carpathians System. In: European Geosciences Union, *Stephan Mueller Special Publications*, vol.3, pp.29–40.

Li, Z.H., Xu, Z., Gerya, T., & Burg, J.P. (2013). Collision of continental corner from 3-d numerical modeling. *Earth Planet. Sci. Lett.* 380, 98–111. https://doi.org /10.1016/j.epsl.2013.08.034.

Loreto, M.F., Zitellini, N., Ranero, C.R., Palmiotto, C. & Prada, M. (2021). Extensional tectonics during the Tyrrhenian back-arc basin formation and a new morphotectonic map. *Basin Res.* https://doi.org/10.1111/bre.12458.

Lukács, R., Harangi, Sz., Guillong, M., Bachmann, O., Fodor, L., Buret, Y., Dunkl, I., Sliwinski, J., von Quadt, A., Peytcheva, I. & Zimmerer, M. (2018). Early to Mid-Miocene syn-extensional massive silicic volcanism in the Pannonian Basin (East-Central Europe): eruption chronology, correlation potential and geodynamic implications. *Earth Sci. Rev.* 179, 1–19. https://doi.org/10.1016/j.earscirev.2018.02.005.

Mannu, U., Ueda, K., Willett, S. D., Gerya, T. V., & Strasser, M. (2017). Stratigraphic signatures of forearc basin formation mechanisms. *Geochemistry, Geophysics, Geosystems,* 18, 2388–2410. https://doi.org/10.1002/2017GC006810

Matenco, L., & Radivojević, D. (2012). On the formation and evolution of the Pannonian Basin: Constraints derived from the structure of the junction area between the Carpathians and Dinarides, *Tectonics, 31*, TC6007, doi:10.1029/2012TC003206.

Magni, V., van Hunen, J., Funiciello, F. & Faccenna, C. (2012). Numerical models of slab migration in continental collision zones. *Solid Earth* 3, 293–306.

Magni, V., Faccenna, C., van Hunen, J. & Funiciello, F. (2014). How collision triggers backarc extension: insight into Mediterranean style of extension from 3-D nu-merical models. *Geology* 42, 511–514.

Magni, V. (2019). The effects of back-arc spreading on arc magmatism. *Earth and Planetary Science Letters*, 519, 141-151.

Menant, A., Sternai, P., Jolivet, L., Guillou-Frottier, L., & Gerya, T. (2016). 3D numerical modeling of mantle flow, crustal dynamics and magma genesis associated with slab roll-back and tearing: the eastern Mediterranean case. *Earth Planet. Sci. Lett.* 442, 93–107.

Menant, A., Angiboust, S., Gerya, T., Lacassin, R., Simoes, M., & Grandin, R. (2020). Transient stripping of subducting slabs controls periodic forearc uplift. *Nature Communications*, 11, 1823, https://doi.org/10.1038/s41467-020-15580-7

Medialdea, T., Vegas, R., Somoza, L., Vazquez, J.T., Maldonado, A., Díaz-del-Río, V., Maestro, A., Cordoba, D., & Fernandez-Puga, M.C. (2004). Structure and evolution of the "Olistostrome" complex of the Gibraltar Arc in the Gulf of Cadiz (eastern Central Atlantic): evidence from two long seismic cross-sections. *Mar. Geol.* 209, 173–198.

Minelli, L., & Faccenna, C. (2010). Evolution of the Calabrian accretionary wedge (central Mediterranean). *Tectonics, 29*, TC4004.

Moore, G. F., B. B. Boston, M. Strasser, M. B. Underwood, & R. A. Ratliff (2015). Evolution of tectono-sedimentary systems in the KumanoBasin, Nankai Trough forearc, *Mar. Pet. Geol.*, 67, 604–616

Munch, J. (2020). Physical controls on dynamics of spontaneously retreating subduction zones. PhD Thesis, ETH Zurich, Switzerland.

Nicolosi, I., F. Speranza, & M. Chiappini (2006). Ultrafast oceanic spreading of the Marsili basin, southern Tyrrhenian Sea: Evidence from magnetic anomaly analysis, *Geology*, 34(9), 717–720, doi:10.1130/G22555.1.

Noda, A. (2016). Forearc basins: Types, geometries, and relationships to subduction zone dynamics. *GSA Bulletin* 128, 879-895.

Pepe, F., Sulli, A., Bertotti, G., & Cella, F. (2010). Architecture and Neogene to Recent evolution of the western Calabrian continental margin: An upper plate perspective to the Ionian subduction system, central Mediterranean. *Tectonics*, 29, TC3007, doi:10.1029/2009TC002599

Pusok, A., & Kaus, B. (2015). Development of topography in 3-D continental-collision models. *Geochem. Geophys. Geosys.* 16, 1378-1400.

Rosenbaum, G. & Lister G. S. (2004). Neogene and Quaternary rollback evolution of the Tyrrhenian Sea, the Apennines, and the Sicilian Maghrebides, *Tectonics*, 23, TC1013.

Royden, L., Horváth, F., & Burchfiel, B.C. (1982). Transform faulting, extension, and subduction in the Carpathian Pannonian region, *GSA Bulletin*, 93, 717-725.

Schmid, S., D. Bernoulli, B. Fügenschuh, L. Matenco, S. Schefer, R. Schuster, M. Tischler, & Ustaszewski, K. (2008). The Alpine-Carpathian-Dinaridic orogenic system: Correlation and evolution of tectonic units, *Swiss J. Geosci.*, 101, 139–183.

Sengul-Uluocak, E., Pysklywec, R. N., Gogus, O. H., & Ulugergerli, E. U. (2019). Multidimensional Geodynamic Modeling in the Sout heastCarpathians: Upper Mantle Flow-Induced SurfaceTopography Anomalies. *Geochemistry, Geophysics, Geosystems, 20, 3134-3449.*

Shemenda, A.I. (1993). Subduction of the Lithosphere and Back Arc Dynamics: Insights From Physical Modeling. *Journal of Geophysical Research.* 98, 167-185.

Sizova, E., Gerya, T., Brown, M., & Perchuk, L.L. (2010). Subduction styles in the Precambrian: insight from numerical experiments. *Lithos*, 116, 209-229.

Sobolev, S. V., & Brown, M. (2019). Surface erosion events controlled the evolution of plate tectonics on Earth. *Nature*, 570(7759), 52. https://doi.org/10.1038/s41586-019-1258-4

Spakman W., & Wortel R. (2004). A Tomographic View on Western Mediterranean Geodynamics. In: Cavazza W., Roure F., Spakman W., Stampfli G.M., Ziegler P.A. (eds) The TRANSMED Atlas. The Mediterranean Region from Crust to Mantle. Springer, Berlin, Heidelberg. https://doi.org/10.1007/978-3-642-18919-7_2

Tackley, P.J. (2000). Mantle convection and plate tectonics: toward an integrated physical and chemical theory. *Science* 288, 2002–2007.

Tari, G., Dovenyi, P., Dunkl, I., Horvath, F., Lenkey, L., S¸tefanescu, M., Szafian, P., & Toth, T. (1999). Lithospheric structure of the Pannonian basin derived from seismic, gravity and geothermal data. In: Durand, B., Jolivet, L., Horvath, F., Serrane, M. (Eds.), The Mediterranean Basins: Extension Within the Alpine Orogen. In: *Geol. Soc. (Lond.) Spec. Publ.*, vol.156, pp.215–250.

Tilita, M., Matenco, L., Dinu, C., Ionescu, L., & Cloetingh, S. (2013). Understanding the kinematic evolution and genesis of a back-arc continental "sag" basin: The Neogene evolution of the Transylvanian Basin. *Tectonophysics*, 602, 237–258. https://doi.org/10.1016/j.tecto.2012.12.029

Torne, M., Fernandez, M., Comas, M.C. & Soto, J. I. (2000). Lithospheric Structure Beneath the Alboran Basin: Results from 3D Gravity Modeling and Tectonic Relevance, *J. Geophys. Res.* 105, 3209-3228.

Toth, J., & Gurnis, M. (1998). Dynamics of subduction initiation at preexisting fault zones. *J. Geophys. Res.* 103 (B8), 18,053–18,067.

Ustaszewski, K., S. Schmid, B. Fügenschuh, M. Tischler, E. Kissling, & W. Spakman (2008). A map-view restoration of the Alpine-Carpathian-Dinaridic system for the early Miocene, *Swiss, J. Geosci.*, 101, 273–294, doi:10.1007/s00015-008-1288-7.

van Hunen, J., van den Berg, A. & Vlaar, N. J. (2000). A thermo-mechanical model of horizontal subduction below an overriding plate. *Earth and Planetary Science Letters*, 182, 157-169.

van Hunen, J., van den Berg, A. P., & Vlaar, N. J. (2004). Various mechanisms to induce present-day shallow flat subduction and implications for the younger Earth: a numerical parameter study. *Physics of the Earth and Planetary Interiors*, 146, 179-194.

Vergés, J., Fernàndez, M. (2012). Tethys–Atlantic interaction along the Iberia–Africa plate boundary: the Betic–Rif orogenic system. *Tectonophysics* 579, 144–172.

Villasenor A, Chevrot S, Harnafi M, Gallart J, Pazos A, Serrano I, et al. (2015). Subduction and volcanism in the Iberia-North Africa collision zone from tomographic images of the upper mantle. *Tectonophysics* 663: 238–249

Vogt, K., Gerya, T.V., & Castro A. (2012). Crustal growth at active continental margins: numerical modeling. *Physics of the Earth and Planetary Interiors*, 192, 1-20.

Wallace, L.M., Ellis, S. & Mann, P. (2009). Collisional model for rapid fore-arc block rotations, arc curvature, and episodic back-arc rifting in subduction settings. *Geochem. Geophys. Geosyst.* 10, Q05001. https://doi .org /10 .1029 /2008GC002220.

Whipple, K., (2009). The influence of climate on the tectonic evolution of mountain belts. *Nature Geosci.* 2, 97-104.

Wolf, S.G., & Huismans R.S. (2019). Mountain Building or Backarc Extension in Ocean-Continent Subduction Systems: A Function of Backarc Lithospheric Strength and Absolute Plate Velocities. *Journal of Geophysical Research: Solid Earth*, 124, 7461–7482. https://doi.org/10.1029/2018JB017171

Wortel, M.J.R. & Spakman, W. (2000). Subduction and slab detachment in the Mediterranean–Carpathian region. *Science* 209, 1910–1917.

Yang, S., Li, Z-H., Wan, B., Chen, L., & Kaus, B. (2021). Subduction-Induced Back-Arc Extension Versus Far-Field Stretching: Contrasting Modes for Continental Marginal Break-Up. *Geochemistry, Geophysics, Geosystems*, 22, e2020GC009416. https://doi.org/10.1029/2020GC009416

Zhong, S. & Gurnis, M. (1992). Viscous flow model of a subduction zone with a faulted lithosphere: long and short wavelength topography, gravity and geoid, *Geophys. Res. Lett.,* 19, 1891-1894.

Zhong, S., & Gurnis, M. (1994). Role of plates and temperature-dependent viscosity in phase change dynamics, *Journal of Geophysical Research*, 99, 15903-15917.

Zito, G., Mongelli, F., de Lorenzo, S. & Doglioni C. (2003). Heat flow and geodynamics in the Tyrrhenian Sea, *Terra Nova*, 15, 425-432.